J. Fluid Mech. (2011), *vol.* 679, *pp.* 315–342.
doi:10.1017/jfm.2011.140

Non-normality and internal flame dynamics in premixed flame–acoustic interaction

PRIYA SUBRAMANIAN† AND R. I. SUJITH

Department of Aerospace Engineering, Indian Institute of Technology Madras, Chennai 600036, India

(Received 5 April 2010; revised 1 January 2011; accepted 16 March 2011;
first published online 13 May 2011)

This paper investigates the non-normal nature of premixed flame–acoustic interaction. The thermoacoustic system is modelled using the acoustic equations for momentum and energy, together with the equation for the evolution of the flame front obtained from the kinematic *G*-equation. As the unsteady heat addition acts as a volumetric source, the flame front is modelled as a distribution of monopole sources. Evolutions of the system are characterized with a measure of energy due to fluctuations. In addition to the acoustic energy, the energy due to fluctuations considered in the present paper accounts for the energy of the monopole sources. The linearized operator for this thermoacoustic system is non-normal, leading to non-orthogonality of its eigenvectors. Non-orthogonal eigenvectors can cause transient growth even when all the eigenvectors are decaying. Therefore, classical linear stability theory cannot predict the finite-time transient growth observed in non-normal systems. In the present model, the state space variables include the monopole source strengths in addition to the acoustic variables. Inclusion of these variables in the state space is essential to account for the transient growth due to non-normality. A parametric study of the variation in transient growth due to change in parameters such as flame location and flame angle is performed. In addition to projections along the acoustic variables of velocity and pressure, the optimal initial condition for the self-evolving system has significant projections along the strength of the monopole distribution. Comparison of linear and corresponding nonlinear evolutions highlights the role of transient growth in subcritical transition to instability. The notion of phase between acoustic pressure and heat release rate as an indicator of stability is examined.

Key words: aeroacoustics, flames, reacting flows

1. Introduction

Stringent emission requirements drive operating conditions of premixed gas turbines and combustors to the lean regime. However, lean premixed combustion has been shown to be particularly susceptible to combustion instability (Annaswamy *et al.* 1997; Lieuwen & Zinn 1998). Combustion instabilities can be defined as self-sustaining oscillations which arise from the coupling between a flame and the acoustic field in the combustor. Fluctuating heat release rate from combustion has long been acknowledged as a source of sound (Lighthill 1952). The acoustic waves produced by combustion can get reflected at the boundaries and again interact with the combustion process to produce further unsteady heat release, thereby forming a feedback loop.

† Email address for correspondence: iitm.priya@gmail.com

These interactions can occur due to modulations of the flame surface area (Boyer & Quinard 1990), equivalence ratio (Lieuwen & Zinn 1998) or burn rate (Wu *et al.* 2003). These interactions can also occur indirectly through coherent vortical structures (Poinsot *et al.* 1987). Many extensive review articles detail the approaches to modelling (Markstein 1964; Coats 1996; Candel 2002; Lieuwen 2003) and controlling combustion instabilities (McManus, Poinsot & Candel 1993; Dowling & Morgens 2005).

A simple model for the premixed flame can be obtained using a kinematic approach to track the flame front evolution. Boyer & Quinard (1990) investigated the dynamics of an anchored premixed flame in the linear regime using a kinematic front tracking equation. Fleifil *et al.* (1996) developed a kinematic model for an axisymmetric premixed flame stabilized in a tube subjected to one-dimensional acoustic excitation. Fluctuations in the surface area of the flame were correlated with heat release rate oscillations. The transfer function characteristics of the premixed flame front have been determined analytically (Schuller, Durox & Candel 2003).

Dowling (1997) proposed a nonlinear model for the heat release response, which saturates when the acoustic velocity amplitude at the flame holder approaches the mean flow velocity. Lieuwen (2005) showed that the nonlinear effects were more dominant for higher Strouhal numbers and flatter flames. Experimental investigations of the nonlinear response of a ducted, conical, laminar premixed flame (Karimi *et al.* 2009) and an ensemble of anchored premixed flames (Noiray *et al.* 2006) subjected to acoustic excitation of varying amplitudes were performed to characterize the transfer function of the premixed flame. Noiray *et al.* (2008) used the amplitude-dependent transfer functions to investigate the stability of the coupled thermoacoustic system using the describing function approach.

These investigations were focused on describing the heat release rate characteristics of the premixed flame in terms of a linear transfer function or a describing function. The obtained response function for the flame is then used as the source in the acoustic energy equation to evaluate the stability of the thermoacoustic system. In the above frequency domain analysis, the transient response of the premixed flame to acoustic velocity perturbations is not captured. However, transient effects can cause significant change in the prediction of system dynamics (Mariappan & Sujith 2010). Therefore, the model of a ducted premixed flame used to investigate thermoacoustic instability must be capable of capturing transient effects.

Annaswamy *et al.* (1997) included the dynamics of premixed flame in the investigation of active control of thermoacoustic instability. Furthermore, Dowling (1999) used the front-tracking equation to model the evolution of a premixed flame in the investigation of the thermoacoustic instability in a ducted premixed flame. The use of an evolution equation to describe the premixed flame includes the transient effects, and hence in the present investigation, this approach is adopted. The equations for the acoustic field are evolved together with the front-tracking equation for the flame.

Annaswamy *et al.* (1997) also discussed the importance of linear coupling between the Galerkin modes in model-based active control design of a ducted premixed flame. They developed a thermoacoustic model for a bench-top premixed combustor and demonstrated that the Galerkin modes were linearly coupled to the thermoacoustic system, both in the presence and absence of an external actuator. It was also shown that the response of the thermoacoustic system to external actuation depends strongly on this linear coupling.

For classical acoustic boundary conditions (e.g. open or closed end) and in the absence of heat addition (e.g. combustion), the eigenmodes in a resonator are normal. Nicoud *et al.* (2007) have shown that the presence of a source of unsteady heat

release and non-trivial boundary conditions can make the eigenmodes non-orthogonal. Non-normality is a property of the operator governing the linear dynamics of a system such that it does not commute with its adjoint (Schmid & Henningson 2001). Non-normal systems have non-orthogonal eigenvectors and can exhibit transient growth (i.e. finite time growth) even when eigenvalues indicate asymptotic stability. Balasubramanian & Sujith (2008*a*) demonstrated that the presence of a fluctuating heat source renders the resulting thermoacoustic system non-normal.

Subcritical bifurcation in thermoacoustic systems was first observed in solid rocket motors (Bloomshield *et al.* 1997). This type of stability transition which is dependent on the amplitude of initial condition is referred to as 'triggering' by the combustion instability community (Wicker *et al.* 1996). A simple thermoacoustic system such as the Rijke tube has been shown to display subcritical bifurcations both in numerical simulations (Matveev 2003*b*; Subramanian *et al.* 2010) and in experiments (Matveev 2003*b*). Transient growth due to non-normality can play a significant role in causing triggering from a small but finite-amplitude initial condition.

Triggering from a small-amplitude initial condition and shift in dominant mode during evolution were demonstrated for a simplified model of a Rijke tube (Balasubramanian & Sujith 2008*b*), for a ducted Burke–Schumann flame with infinite rate chemistry (Balasubramanian & Sujith 2008*a*). Two possible routes to triggering, one from a large-amplitude initial condition and the other from small but finite amplitude which causes non-normal transient growth, were demonstrated for the case of a solid rocket motor with homogeneous propellant (Mariappan & Sujith 2010). The lowest initial energy required to trigger instability in a model for a horizontal Rijke tube was determined using the optimization method of adjoint looping (Juniper 2010).

The energy due to fluctuations in a system forms a measure or norm to characterize the transient growth in the system. Disturbance energy is the energy associated with fluctuations superimposed over a base flow. It should account for contributions from all the constituent phenomena in the system. Kinetic energy was chosen as the natural measure to describe transient growth due to non-normality for incompressible fluid flows (Schmid & Henningson 2001). However, there has been no such consensus on the appropriate expression for disturbance energy for compressible reacting flows.

Chu (1964) derived the energy of a small disturbance in a viscous compressible flow which included the energy due to entropy fluctuations in addition to the energy due to pressure and velocity fluctuations. Morfey (1971) derived a measure for the energy due to small fluctuations with an irrotational base flow. Myers (1991) relaxed the restrictive assumptions regarding the nature of the base flow and perturbation amplitude and derived a measure for disturbance energy in a general steady flow. In addition to the classical acoustic energy, this measure accommodates the energy associated with fluctuations in vorticity and entropy. In compressible flows, the spatial average of the rate of pressure related work or compression work does not contribute to the evolution of energy density (Mack 1969; Chagelishvili, Rogava & Segal 1994; Farrell & Ioannou 2000). Myers's measure for disturbance energy can be further modified to account for this conservative nature of compression work (Bakas 2009).

Nicoud & Poinsot (2005) argued that the Rayleigh criterion gives an incomplete description of the significant sources of fluctuating energy in a flow with combustion. Giauque *et al.* (2006) extended the expression for disturbance energy from Myers to incorporate species and heat release terms in the energy of fluctuations. In addition to the expression for the acoustic energy, the energy measure chosen to study the non-normal nature of thermoacoustic instability in solid rocket motors included the entropy fluctuations within the propellant (Mariappan & Sujith 2010).

Evidently, it is critical to define the energy in a disturbance depending on the system under consideration. Therefore, there is a need to identify a measure to quantify the disturbance energy in premixed flame–acoustic interaction.

In this paper the interaction of a longitudinal acoustic field in a duct with the unsteady heat release from a laminar premixed flame is analysed. A low-Mach-number laminar inviscid flow is assumed and the acoustic equations for momentum and energy are used to describe the evolution of the acoustic field in the duct. All reaction parameters are frozen by assuming a constant value for the laminar flame speed. An axisymmetric wedge flame is modelled as a kinematic flame front which separates the unburnt mixture and the products of combustion (Kerstein, Ashurst & Williams 1988).

The objective of this paper is to arrive at an expression for the energy due to fluctuations and use it to characterize the non-normal nature of the premixed flame–acoustic interaction. We investigate the effect of system parameters such as flame location and flame angle on transient growth due to non-normality. We also examine the possibility of subcritical transition to instability from a small yet finite-amplitude initial condition. The organization of the rest of the paper is as follows. In § 2 the *G*-equation governing the premixed flame model is discussed. Section 3 explains the governing equations which describe the acoustic field within the duct. Section 4 explains the modelling of the flame front in terms of a distribution of acoustic monopole sources. An expression for the total energy due to fluctuations in a premixed flame–acoustic system is derived in § 5. The equations governing the linear and nonlinear evolutions are described in § 6. Section 7 discusses the results and § 8 summarizes the important results.

2. Combustion model

The laminar premixed flame is modelled as a thin wrinkled interface which separates the unburnt mixture and the burnt products of combustion (Kerstein *et al.* 1988). In this kinematic approach, the governing differential equation for the dynamics of premixed flame is given by the *G*-equation. The scalar variable G can be related to the signed distance of the flame front from its unperturbed location $\tilde{\xi}'(\tilde{X})$ along the direction $\tilde{Y}$ as shown in figure 1. The flame is along the axes $(\tilde{X}, \tilde{Y})$ stabilized in a duct with purely axial velocity $\tilde{u}$ along $\tilde{y}$ in the $(\tilde{x}, \tilde{y})$ coordinate axes. The two coordinate systems are related by the following transformations where α is the angle which the unperturbed flame makes with the flow:

$$\tilde{x} = \tilde{X}\sin\alpha - \tilde{\xi}'\cos\alpha \text{ and } \tilde{y} = \tilde{X}\cos\alpha + \tilde{\xi}'\sin\alpha. \tag{2.1}$$

Both the coordinates axes are retained, since even when the acoustic field in the duct is along the $(\tilde{x}, \tilde{y})$ axis, the flame front is linearized about the $(\tilde{X}, \tilde{Y})$ axis. Using the above transformations and decomposing the axial velocity into its mean and perturbed values, the *G*-equation for the flame front can be rewritten as the front-tracking equation (Fleifil *et al.* 1996). For the geometry of an axisymmetric wedge flame stabilized on a wire adapted from Schuller *et al.* (2003), the front-tracking equation in the flame fixed coordinate axes is as follows:

$$\frac{\partial\tilde{\xi}'}{\partial\tilde{t}} + (\tilde{\bar{u}} + \tilde{u}')\cos\alpha\frac{\partial\tilde{\xi}'}{\partial\tilde{X}} - (\tilde{\bar{u}} + \tilde{u}')\sin\alpha = -\tilde{S}_L\sqrt{1 + \left(\frac{\partial\tilde{\xi}'}{\partial\tilde{X}}\right)^2}. \tag{2.2}$$

Here the tildes denote dimensional values and primes indicate fluctuating quantities. Also, $(\tilde{\bar{u}} + \tilde{u}')\cos\alpha$ is the component of axial velocity parallel to the flame front,

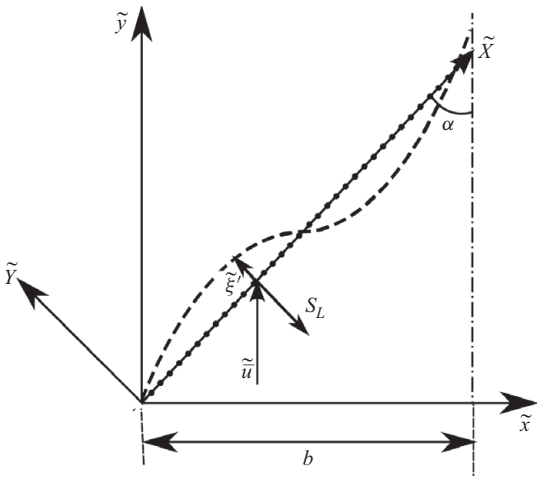

FIGURE 1. Geometry of axisymmetric wedge flame stabilized on a wire. Here $\tilde{\xi}'$ is the displacement of the instantaneous flame shape from the unperturbed flame shape, α is the flame angle, S_L is the laminar flame speed and $\tilde{u}$ is the mean flow.

$(\tilde{\bar{u}} + \tilde{u}')\sin\alpha$ is the component of axial velocity perpendicular to the flame front and $\tilde{S}_L$ is the laminar flame speed.

The effect of all reaction parameters is distilled into the laminar flame speed, which is considered to be only a function of the equivalence ratio of the unburnt mixture. A methane–air flame is considered and for a given equivalence ratio (ϕ) the laminar flame speed ($\tilde{S}_L$) is obtained using the following relation from You, Huang & Yang (2005), where $J = 0.6079\ \mathrm{m\,s^{-1}}$:

$$\tilde{S}_L(\phi) = J(\phi^{-2.554}\exp[-7.31(\phi - 1.23)^2]). \tag{2.3}$$

Equation (2.2) is nonlinear and describes the combustion response of a premixed flame when subjected to a velocity perturbation. Linearizing it, the following equation is obtained:

$$\frac{\partial\tilde{\xi}'}{\partial\tilde{t}} = \tilde{u}'\sin\alpha - \tilde{\bar{u}}\cos\alpha\frac{\partial\tilde{\xi}'}{\partial\tilde{X}}. \tag{2.4}$$

The length scale used for non-dimensionalization is the length of the flame ($b/\sin\alpha$), where b is the radius of the burner. The velocity scale chosen is the mean velocity of the flow ($\bar{u}$). The time scale for non-dimensionalization is derived from the length and velocity scales as shown in (2.5) to derive the non-dimensional time in the combustion scale t_c. The non-dimensional linear (2.6) and nonlinear (2.7) front-tracking equations are obtained as follows:

$$y = \tilde{y}\sin\alpha/b, \quad \bar{u} = \tilde{\bar{u}}/\tilde{\bar{u}} = 1, \quad t_c = \tilde{t}/(b/\bar{u}\sin\alpha), \tag{2.5}$$

$$\frac{\partial\xi'}{\partial t_c} = u'\sin\alpha - \cos\alpha\left(\frac{\partial\xi'}{\partial X}\right), \tag{2.6}$$

$$\frac{\partial\xi'}{\partial t_c} = (1+u')\sin\alpha - (1+u')\cos\alpha\left(\frac{\partial\xi'}{\partial X}\right) - \sin\alpha\sqrt{1+\left(\frac{\partial\xi'}{\partial X}\right)^2}. \tag{2.7}$$

The above equations are first order in time and space and therefore require an initial condition and a boundary condition for their solution. The flame is assumed to be

anchored at the base and the other end is left free to move. The resulting system can be evolved from a prescribed initial condition using a numerical integration scheme.

The shape function $\xi'(X,t)$ is smooth for small amplitude perturbations in the linear regime. Therefore, in the linear regime, the gradient term is expanded using a first-order backward-difference formula. However, the shape function $\xi'(X,t)$ can become significantly distorted and can even display a discontinuity in slope at high perturbation amplitudes (Dowling 1999). Therefore, it becomes necessary to calculate the spatial derivative of the shape function to high accuracy using a high-resolution method. The high-resolution scheme used to capture the highly oscillatory solution of the *G*-equation is the weighted essentially non-oscillatory (WENO) scheme of the third order (Jiang & Shu 1996; Schuller *et al.* 2003). The implementation details are given in Appendix A. The above formulation enables us to achieve fifth-order accuracy in smooth regions and third-order accuracy in the discontinuous regions for the spatial derivative of the flame shape.

The flame front area is calculated for the geometry of the flame front from its instantaneous position for nonlinear and linearized equations as per the geometry of the flame front. For the geometry of an axisymmetric wedge flame stabilized on a wire, as given in figure 1, the flame shape at the unperturbed state can be approximated by an inverted cone. The nonlinear and linear expressions for the total surface area of the perturbed flame front are given as follows:

$$\text{nonlinear}: \quad A(t_c) = 2\pi \int_{X=0}^{X=1} (X\sin\alpha - \xi'\cos\alpha)\sqrt{1+\left(\frac{\partial \xi'}{\partial X}\right)^2}\,\mathrm{d}X, \tag{2.8}$$

$$\text{linear}: \quad A(t_c) = 2\pi \int_{X=0}^{X=1} (X\sin\alpha - \xi'\cos\alpha)\,\mathrm{d}X. \tag{2.9}$$

The linear relation for the change in the surface area of the flame due to change in the flame shape is obtained with the relation (2.9). Dimensionally, this relation can be written as

$$\tilde{A}(t_c) = \frac{2\pi b^2}{\sin^2\alpha} \int_{X=0}^{X=1} (X\sin\alpha - \xi'\cos\alpha)\,\mathrm{d}X. \tag{2.10}$$

The unperturbed flame shape is obtained from the above relation when $\xi' = 0$ such that the dimensional surface area of the unperturbed flame $\tilde{\bar{A}}(t_c)$ is given by the following expression:

$$\tilde{\bar{A}}(t_c) = \frac{2\pi b^2}{\sin^2\alpha} \int_{X=0}^{X=1} X\sin\alpha\,\mathrm{d}X = \frac{\pi b^2}{\sin\alpha}. \tag{2.11}$$

Retaining the expression with the integral and subtracting it from the expression for the total surface area of the flame given in (2.10), we obtain the linear expression for the fluctuating surface area as

$$\tilde{A}'(t_c) = \frac{-2\pi b^2\cos\alpha}{\sin^2\alpha} \int_{X=0}^{X=1} \xi'\,\mathrm{d}X. \tag{2.12}$$

Following the kinematic flame model of Fleifil *et al.* (1996) with constant flame speed and no equivalence ratio fluctuations, the evolution of heat release fluctuations imitates the evolution of the area ratio such that $\dot{\tilde{q}}'/\dot{\tilde{\bar{q}}} = \tilde{A}'/\tilde{\bar{A}}$, or as given below:

$$\dot{\tilde{q}} = \dot{\tilde{\bar{q}}} + \dot{\tilde{q}}' = \rho_0 S_L \Delta q_R (\tilde{\bar{A}} + \tilde{A}'). \tag{2.13}$$

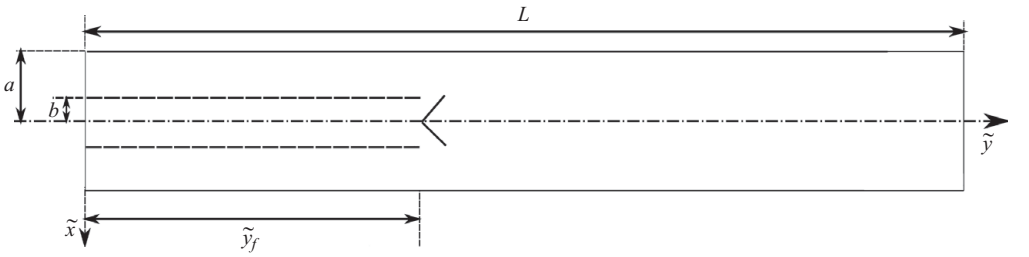

FIGURE 2. Geometry of the coupled system with an axisymmetric wedge flame stabilized on a wire. Here L is the length of the duct, (b/a) is the ratio of burner to duct radius and $\tilde{y}_f$ is the flame location along the length of the duct.

Here, ρ_0 is the density of the unburnt mixture in $\mathrm{kg\,m^{-3}}$, S_L is the laminar flame speed in $\mathrm{m\,s^{-1}}$ and Δq_R is the heat released per unit mass of the mixture in $\mathrm{J\,kg^{-1}}$ at equivalence ratio ϕ and is obtained for a methane–air mixture from You *et al.* (2005) as follows:

$$\Delta q_R(\phi) = \begin{cases} \dfrac{2.9125\times10^6\phi}{1+0.05825\phi}, & \phi \leqslant 1 \\ \dfrac{2.9125\times10^6}{1+0.05825\phi}, & \phi > 1 \end{cases}, \quad \mathrm{J\,kg^{-1}}. \tag{2.14}$$

The fluctuating part of the dimensional heat release rate can be calculated from the fluctuating surface area using the relation given in (2.13) for a specified equivalence ratio. Thus,

$$\dot{\tilde{q}}' = \rho_0 S_L \Delta q_R \tilde{A}'(t) = \frac{-2\pi\cos\alpha\ \rho_0 S_L \Delta q_R b^2}{\sin^2\alpha} \int_{X=0}^{X=1} \xi'\,\mathrm{d}X. \tag{2.15}$$

3. Model for the coupled thermoacoustic system

The coupled thermoacoustic system considered here is given in figure 2. It consists of the acoustic field within a duct open at both ends and a compact premixed flame located within it. A laminar inviscid flow with Mach number (M) approaching zero is assumed (Nicoud & Wieczorek 2009). In order to simplify the analysis, a constant density assumption is made such that the mean density ($\tilde{\rho}_0$) and the speed of sound in the unburnt mixture ($\tilde{c}_0$) are assumed to be constant throughout the duct. The flame is treated as a compact source and the heat release rate distribution along the duct can be represented by a Dirac delta function. The location of the flame is the point of attachment of the flame front to the anchoring wire, i.e. at $\tilde{y} = \tilde{y}_f$.

The acoustic wave propagation on either side of the compact source within the duct can be assumed to be linear even when the nonlinear dependence of the heat release rate on velocity fluctuations is retained. This is because the amplitudes of the acoustic pressure fluctuations in the present thermoacoustic system are not significant enough to introduce nonlinear gas-dynamic effects (Dowling 1997). Below the cut-on frequency, only the axial modes of sound propagate in the duct. Therefore, the acoustic quantities are assumed to vary only axially. The one-dimensional acoustic equations for momentum and energy in the limit of $M \to 0$ are used in the present analysis. They are given, along with the scales of non-dimensionalization

(Balasubramanian & Sujith 2008*a*), as follows:

$$y_a = \tilde{y}/L, \quad u = \tilde{u}/\bar{u}, \quad t = \tilde{t}c_0/L, \quad p = \tilde{p}/\bar{p}, \quad \dot{q}'_f = \dot{\tilde{q}}'_f/\rho_0 c_0^3, \quad \delta = L\tilde{\delta}, \tag{3.1}$$

$$\gamma M \frac{\partial u'}{\partial t} + \frac{\partial p'}{\partial y_a} = 0, \tag{3.2}$$

$$\frac{\partial p'}{\partial t} + \gamma M \frac{\partial u'}{\partial y_a} = (\gamma - 1)\frac{\dot{\tilde{q}}'_f}{\rho_0 c_0^3}\delta(y_a - y_{fa}), \tag{3.3}$$

where γ is the ratio of specific heats, p' is the non-dimensional acoustic pressure, u' is the non-dimensional acoustic velocity, $\dot{\tilde{q}}'_f$ is the heat release rate fluctuations averaged over the cross-sectional area of the duct, L is the duct length and the compact heat source is represented by the Dirac delta function $\delta(y_a - y_{fa})$. In this paper, the superscript tilde denotes dimensional quantities and quantities without tilde are non-dimensional. The subscript '*a*' denotes that the variable has been non-dimensionalized with respect to the acoustic scale.

The heat release rate fluctuation averaged over the cross-sectional area of the duct ($\tilde{A}_{CS} = \pi a^2$) is given as $\dot{\tilde{q}}'_f = \dot{\tilde{q}}'/\tilde{A}_{CS}$. Therefore, the expression for the fluctuating heat release rate per unit area for the linearized model can be written using (2.15) as

$$\dot{\tilde{q}}'_f = \frac{\rho_0 S_L \Delta q_R \tilde{A}'(t)}{\tilde{A}_{CS}} = -2\cot\alpha\ \rho_0 S_L \Delta q_R \left(\frac{b^2}{a^2 \sin\alpha}\right) \int_{X=0}^{X=1} \xi'\, \mathrm{d}X. \tag{3.4}$$

Defining the constant $\Omega = -(L/\rho_0 c_0^3)(2\cot\alpha \rho_0 S_L \Delta q_R)(b^2/a^2 \sin\alpha)$, the equation for the non-dimensional heat release rate fluctuations per unit area of the duct can be written as follows:

$$\dot{q}'_f = \left(\frac{L}{\rho_0 c_0^3}\right) \dot{\tilde{q}}'_f = \Omega \int_{X=0}^{X=1} \xi'\, \mathrm{d}X. \tag{3.5}$$

Implementing the Galerkin technique for the acoustic field, the acoustic equations for momentum and energy are converted into a set of ordinary differential equations (Meirovitch 1967; Zinn & Lores 1971). The appropriate basis functions which satisfy the boundary conditions for the acoustic field within a duct open at both ends are chosen as follows:

$$u' = \sum_{j=1}^{N} \cos(j\pi y_a)\, \eta_j(t) \quad \text{and} \quad p' = -\sum_{j=1}^{N} \frac{\gamma M}{j\pi} \sin(j\pi y_a)\, \dot{\eta}_j(t). \tag{3.6}$$

A mode-dependent damping is introduced as given by Matveev (2003*a*) in the acoustic energy equation, where the expression for the damping coefficient (ζ_j) is given by

$$\zeta_j = \frac{1}{2\pi}\left(c_1 j + c_2 \sqrt{\frac{1}{j}}\right). \tag{3.7}$$

Here, c_1 is representative of the losses due to radiation from the open ends and c_2 represents the acoustic boundary layer losses (Sterling & Zukoski 1991). The resulting system of ordinary differential equations which describes the evolution of the acoustic field for the system with damping is as follows:

$$\frac{\mathrm{d}\eta_j}{\mathrm{d}t} = j\pi \left(\frac{\dot{\eta}_j}{j\pi}\right), \tag{3.8}$$

$$\frac{\mathrm{d}}{\mathrm{d}t}\left(\frac{\dot{\eta}_j}{j\pi}\right) = -j\pi\eta_j - 2\zeta_j j\pi \left(\frac{\dot{\eta}_j}{j\pi}\right) - \frac{2(\gamma - 1)}{\gamma M}\dot{q}'_f(t)\sin(j\pi y_{fa}). \tag{3.9}$$

The acoustic equations are linear and the nonlinearity in the system is due to the heat release rate term. Therefore, evolutions of the linear or nonlinear system can both be investigated by including the appropriate model for the heat release rate in the above equations.

4. Modelling the flame front as a distribution of monopole sources

The flame front can be represented as a source of sound using Lighthill's acoustic analogy (1952). Unsteady heat addition from the flame at constant pressure causes a corresponding unsteady expansion of the fluid. Across a one-dimensional flame with area A_f, this dilatation term leads to a velocity jump of $\delta u'_f$, resulting in an instantaneous value of volume flow rate $A_f \delta u'_f$ (Chu & Kovasznay 1957; Wu *et al.* 2003). This dilatation can be represented as the sum of source strengths of a distribution of monopole sources of sound, with source strength per unit length S along the flame front (Morse & Ingard 1968; Dowling & Pierce 1983; Howe 2003). Thus, the laminar flame front is represented by a distribution of monopole sources of sound (van Kampen 2006).

The flame front is discretized into P flame elements each of equal length $\Delta\tilde{X}$, each of which represents an acoustic monopole source of strength $\tilde{S}_i \Delta\tilde{X}$. The monopole strength per unit length $\tilde{S}_i$ can be non-dimensionalized as follows:

$$S_i = \frac{1}{\gamma \bar{u} L} \tilde{S}_i. \tag{4.1}$$

In the rest of this section, we derive the energy due to heat release rate fluctuations of the flame front in terms of monopole strength averaged over the cross-sectional area of the duct. As the initial step, (3.5) can be rewritten to linearly relate the local flame displacement to the non-dimensional heat release rate fluctuation per unit area as follows:

$$\dot{q}'_f = \sum_{i=1}^{P} \dot{q}'_{fi} = \Omega \sum_{i=1}^{P} f_i \xi'_i \Delta X, \tag{4.2}$$

given that we denote Ω as defined before (3.5) and f_i are the weight factors corresponding to the trapezoidal integration formula as given below:

$$f_i = \begin{cases} \frac{1}{2}, & i = 1 \quad \text{and} \quad P, \\ 1, & i \neq 1 \quad \text{or } P. \end{cases} \tag{4.3}$$

The integration of the acoustic equation for energy given by (3.3) across the heat source relates the acoustic velocity gradient to the heat source given in (4.4)–(4.8):

$$\int_{y_f^-}^{y_f^+} \left(\frac{\partial p'}{\partial t} + \gamma M \frac{\partial u'}{\partial y_a} \right) \mathrm{d}V_c = \int_{y_f^-}^{y_f^+} (\gamma - 1) \dot{q}'_f \delta(y_a - y_{fa}) \, \mathrm{d}V_c. \tag{4.4}$$

Here y_f^- and y_f^+ are the locations just upstream and downstream of the flame front and the subscript c denotes the combustion zone. The contribution from the acoustic pressure term vanishes for a compact source as $\mathrm{d}V_c \to 0$. Applying Gauss's divergence theorem to the acoustic gradient term, we can rewrite the left-hand side of (4.4) as follows:

$$\gamma M \int_{y_f^-}^{y_f^+} \left(\frac{\partial u'}{\partial y_a} \right) \mathrm{d}V_c = \gamma M \int_{S_c} (u' \cdot \hat{n}) \, \mathrm{d}S_c. \tag{4.5}$$

The surface integral is evaluated over a cylindrical area S_c, which encloses the flame and whose lateral surface coincides with that of the duct. Here, $\hat{n}$ denotes the outward normal from the surface.

As the velocity field is assumed to be one-dimensional, the contribution to the integral from the lateral surface vanishes identically. Furthermore, the acoustic velocity is assumed to be uniform across the cross-sectional area of the duct, consistent with a one-dimensional approximation. Therefore, the contribution to this surface integral from the left and right faces of the cylindrical area is $(-A_{CS}u'_{f-})$ and $(A_{CS}u'_{f+})$, respectively, as given by the right-hand term of

$$(\gamma-1)\int_{y_f^-}^{y_f^+}\dot{q}'_f\delta(y_a-y_{fa})\,\mathrm{d}V_c=\gamma M A_{CS}(\delta u'_f). \tag{4.6}$$

Using the one-dimensional approximation, the volume integral on the left-hand-side term in (4.6) is replaced as the product of the cross-sectional area A_{CS} times an integral along the length of the duct,

$$(\gamma-1)\int_{\delta^-}^{\delta^+}\dot{q}'_f\delta(y_a-y_{fa})\,\mathrm{d}V_c=(\gamma-1)A_{CS}\;\dot{q}'_f|_{y_a=y_{fa}}. \tag{4.7}$$

Comparing the right-hand sides of (4.6) and (4.7), the jump in acoustic velocity across the heat source $\delta u'_f$ can be related to the fluctuations in heat release rate as follows:

$$\delta u'_f=\frac{(\gamma-1)}{\gamma M}\;\dot{q}'_f|_{y_a=y_{fa}}. \tag{4.8}$$

The jump in acoustic velocity $\delta u'_{fi}$ across the ith monopole can be related in terms of the monopole strength $S_i\Delta X$ averaged over the cross-sectional area of the duct as given below (Morse & Ingard 1968; Dowling & Pierce 1983; Howe 2003):

$$\delta u'_{fi}=\frac{S_i\Delta X}{A_{CS}}, \tag{4.9}$$

which we will use later in § 5.2 to calculate the energy due to fluctuations in heat release rate.

5. Energy due to fluctuations in a premixed flame–acoustic system

5.1. *Energy in the acoustic field*

The acoustic energy can be written in terms of the acoustic velocity and pressure as follows (Rienstra & Hirschberg 2008):

$$\tilde{E}_a(t)=\frac{1}{2}\int_{\tilde{V}_a}\left[(\rho_0\tilde{u}'^2)+\left(\frac{\tilde{p}'^2}{\rho_0c_0^2}\right)\right]\mathrm{d}\tilde{V}_a=\frac{1}{2}A_{CS}L\int_{y_a=0}^{y_a=1}\left[(\rho_0\tilde{u}'^2)+\left(\frac{\tilde{p}'^2}{\rho_0c_0^2}\right)\right]\mathrm{d}y_a. \tag{5.1}$$

Non-dimensionalizing the above expression with the kinetic energy of the steady-state flow, $\frac{1}{2}\rho_0\bar{u}^2A_{CS}L$, we obtain the expression for non-dimensional acoustic energy as below:

$$E_a(t)=\frac{\tilde{E}_a(t)}{\frac{1}{2}\rho_0\bar{u}^2A_{CS}L}=\int_{y=0}^{y=1}\left[u'^2+\left(\frac{p'}{\gamma M}\right)^2\right]\mathrm{d}y_a. \tag{5.2}$$

We expand the acoustic variables in terms of the Galerkin basis functions as given in (3.6) and integrate over the acoustic domain. Making use of their orthogonality

property, the expression for acoustic energy can be modified as follows:

$$E_a(t) = \frac{1}{2}\sum_{j=1}^{N}\left[\eta_j(t)^2 + \left(\frac{\dot{\eta}_j(t)}{j\pi}\right)^2\right]. \tag{5.3}$$

5.2. *Energy due to fluctuations in heat release rate*

In § 4, the unsteady heat addition at the flame front was related to unsteady expansion of the fluid across it. The energy due to dilatation at the monopole distribution $\tilde{E}_f$ (Morse & Ingard 1968) is written in the dimensional form as follows:

$$\tilde{E}_f(t) = \frac{1}{2}\int_{\tilde{V}_a}\left[\rho_0\sum_{i=1}^{P}(\delta\tilde{u}'_{fi})^2\right]\mathrm{d}\tilde{V}_a = \frac{1}{2}A_{CS}L\int_{y_a=0}^{y_a=1}\left[\rho_0\sum_{i=1}^{P}(\delta\tilde{u}'_{fi})^2\right]\mathrm{d}y_a. \tag{5.4}$$

Non-dimensionalizing the above the kinetic energy of the steady-state flow, $\frac{1}{2}\rho_0\bar{u}^2A_{CS}L$, we obtain the non-dimensional expression for the energy of the monopole distribution as

$$E_f(t) = \frac{\tilde{E}_f(t)}{\frac{1}{2}\rho_0\bar{u}^2A_{CS}L} = \sum_{i=1}^{P}(\delta u'_{fi})^2. \tag{5.5}$$

Using (4.9), we can rewrite the expression for energy E_f in terms of monopole strengths to obtain

$$E_f(t) = \sum_{i=1}^{P}\left[\frac{S_i(t)\Delta X}{A_{CS}}\right]^2. \tag{5.6}$$

The dilatation resulting from heat release rate fluctuations is the energy due to the presence of the flame front which is modelled as a monopole distribution and is given in terms of the monopole strength averaged over the cross-sectional area of the duct. Note that the expression for the fluctuating energy as derived in (5.6) is not the acoustic power of a distribution of monopole sources (Morse & Ingard 1968).

The total energy $E(t)$ due to fluctuations in a premixed flame–acoustic system includes contributions from the acoustic energy and the energy contributed by the monopole distribution arising from the heat release rate fluctuations. Thus, $E(t)$ can be expressed as

$$E(t) = E_a(t) + E_f(t) = \sum_{j=1}^{N}\frac{1}{2}\left[\eta_j(t)^2 + \left(\frac{\dot{\eta}_j(t)}{j\pi}\right)^2\right] + \sum_{i=1}^{P}\left[\frac{S_i(t)\Delta X}{A_{CS}}\right]^2. \tag{5.7}$$

The above expression is proportional to the square of the L^2-norm of the state vector as given in § 6.1.

6. Evolution equations for the premixed flame thermoacoustic system

The time scale used in the non-dimensional front-tracking equation is ($t_c = b/\bar{u}\sin\alpha$), which is different from the time scale used for the acoustic equations for momentum and energy ($t = L/c_0$). In order to evolve both using a single time-marching technique, the time scale of the non-dimensional front-tracking equation is rescaled to the acoustic time scale using the ratio of the time scales as

$$\left(\frac{L}{c_0}\frac{\bar{u}\sin\alpha}{b}\right)\frac{\partial}{\partial t_c} = \frac{\partial}{\partial t}, \tag{6.1}$$

such that the front-tracking equation can be modified as given in (6.4) and (6.10). Also, the flame front is discretized into P different flame elements along its length such that the partial differential equation that governs the flame front evolution can be converted into P ordinary differential equations.

6.1. *Linear analysis*

The coupled system of equations for the premixed flame thermoacoustic system under the linear approximation can be written as follows:

$$\frac{\mathrm{d}\eta_j}{\mathrm{d}t} = j\pi\left(\frac{\dot{\eta}_j}{j\pi}\right), \tag{6.2}$$

$$\frac{\mathrm{d}}{\mathrm{d}t}\left(\frac{\dot{\eta}_j}{j\pi}\right) = -j\pi\eta_j - 2\zeta_j j\pi\left(\frac{\dot{\eta}_j}{j\pi}\right) - \frac{2(\gamma-1)}{\gamma M}\dot{q}'_f(t)\sin(j\pi y_{fa}), \tag{6.3}$$

$$\frac{\mathrm{d}\xi'_i}{\mathrm{d}t} = \left(\frac{L\bar{u}\sin^2\alpha}{c_0 b}\right)\sum_{j=1}^{N}\cos(j\pi y_{fa})\eta_j - \left(\frac{L\bar{u}\sin\alpha\cos\alpha}{c_0 b}\right)\left(\frac{\Delta\xi'}{\Delta X}\right)_i. \tag{6.4}$$

Here, the gradient term $(\Delta\xi'/\Delta X)_i$ in the front-tracking equation in expanded using a first-order backward-difference formula as discussed in § 2.

Equation (6.2) is retained as such, while (6.3) is rewritten in terms of the strength of monopole distribution as follows:

$$\frac{\mathrm{d}}{\mathrm{d}t}\left(\frac{\dot{\eta}_j}{j\pi}\right) = -j\pi\eta_j - 2\zeta_j j\pi\left(\frac{\dot{\eta}_j}{j\pi}\right) - \sqrt{2}\sin(j\pi y_{fa})\sum_{i=1}^{P}H_i. \tag{6.5}$$

With H_i representing the monopole strength averaged over the cross-sectional area of the duct and defining the constants θ_1 and θ_2,

$$H_i = \left(\frac{S_i\Delta X\sqrt{2}}{A_{CS}}\right), \tag{6.6}$$

$$\theta_1 = \left(\frac{(\gamma-1)\Omega\Delta X\sqrt{2}}{\gamma M}\right)\left(\frac{L\bar{u}\sin^2\alpha}{c_0 b}\right) \quad \text{and} \quad \theta_2 = \left(\frac{L\bar{u}\sin\alpha\cos\alpha}{c_0 b\Delta X}\right), \tag{6.7}$$

the flame front evolution (6.4) is converted to (6.8) using relations (4.9) and (4.2):

$$\frac{\mathrm{d}H_i}{\mathrm{d}t} = \theta_1\sum_{j=1}^{N}\cos(j\pi y)\eta_j - \theta_2(H_i - H_{(i-1)}). \tag{6.8}$$

The state vector $\boldsymbol{\chi} = [\eta_1\ \dot{\eta}_1/\pi\ \eta_2\ \dot{\eta}_2/2\pi\ \cdots\ \dot{\eta}_N/N\pi\ H_1\ H_2\ \cdots\ H_P]^{\mathrm{T}}$ is defined such that the square of the L^2-norm of the state vector is proportional to the energy of fluctuations $E(t)$. The ratio of the squares of the L^2-norm of the state vector at time t to that at time $t=0$ gives the normalized energy of fluctuations as follows:

$$\frac{E(t)}{E(0)} = \frac{\left(\sum_{j=1}^{N}\left[\eta_j(t)^2 + \left(\frac{\dot{\eta}_j(t)}{j\pi}\right)^2\right] + \sum_{i=1}^{P}H_i(t)^2\right)}{\left(\sum_{j=1}^{N}\left[\eta_j(0)^2 + \left(\frac{\dot{\eta}_j(0)}{j\pi}\right)^2\right] + \sum_{i=1}^{P}H_i(0)^2\right)}. \tag{6.9}$$

Thus, the set of linear equations which describes the evolution of a premixed flame thermoacoustic system is given by (6.2), (6.5) and (6.8).

6.2. *Nonlinear analysis*

The nonlinear partial differential equation which governs the evolution of the flame front expressed in the acoustic time scale is

$$\frac{\partial \xi'}{\partial t} = \left(\frac{L\bar{u}\sin^2\alpha}{c_0 b}\right)\left(1 + u'_f - \sqrt{1+\left(\frac{\partial \xi'}{\partial X}\right)^2}\right) - \left(\frac{L\bar{u}\sin\alpha\cos\alpha}{c_0 b}\right)(1+u'_f)\left(\frac{\partial \xi'}{\partial X}\right). \tag{6.10}$$

The discretized set of equations for the evolution of the flame front can be written as below for every $i = 1, 2, \ldots, P$, where P is the number of points along the flame front:

$$\frac{\mathrm{d}\xi'_i}{\mathrm{d}t} = \left(\frac{L\bar{u}\sin^2\alpha}{c_0 b}\right)\left(1 + u'_f - \sqrt{1+\left(\frac{\Delta \xi'_i}{\Delta X}\right)^2}\right) - \left(\frac{L\bar{u}\sin\alpha\cos\alpha}{c_0 b}\right)(1+u'_f)\left(\frac{\Delta \xi'_i}{\Delta X}\right). \tag{6.11}$$

Here $(\Delta\xi'_i/\Delta X)$ is the fifth-order-accurate approximation of the spatial derivative using the WENO scheme given in Appendix A. The governing equations for the nonlinear system are the linearized acoustic equations for momentum and energy (6.2) and (6.3) and the nonlinear evolution equation for the premixed flame given in (6.11). In (6.3), the heat release rate is substituted in terms of the flame displacement as

$$\dot{q}'_f = \frac{S_L \Delta q_R}{c_0^3}\left(\frac{2}{\sin\alpha}\int_{X=0}^{X=1}(X\sin\alpha - \xi'\cos\alpha)\sqrt{1+\left(\frac{\partial \xi'}{\partial X}\right)^2}\,\mathrm{d}X - 1\right). \tag{6.12}$$

Two measures are chosen to check the convergence with increasing number of acoustic modes and number of flame elements. The number of acoustic modes is varied in steps of one and the number of flame elements is varied in steps of 25 and the following two relative changes are calculated. The relative changes, due to variation in the number of acoustic modes N, in the maximum transient growth Φ_1 and the average acoustic velocity at the flame for the optimal initial condition Φ_2 are respectively

$$\Phi_1 = \frac{G_{max(N)} - G_{max(N-1)}}{G_{max(N)}} \quad \text{and} \quad \Phi_2 = \frac{u'_{f(N)} - u'_{f(N-1)}}{u'_{f(N)}}. \tag{6.13}$$

The relative changes, due to variation in the number of flame elements P, in the maximum transient growth Ψ_1 and the average acoustic velocity at the flame for the optimal initial condition Ψ_2 are respectively

$$\Psi_1 = \frac{G_{max(P)} - G_{max(P-25)}}{G_{max(P)}} \quad \text{and} \quad \Psi_2 = \frac{u'_{f(P)} - u'_{f(P-25)}}{u'_{f(P)}}. \tag{6.14}$$

Figure 3(*a*) plots the variation of Φ_1 and Φ_2 with a change in the number of acoustic modes N for the case with system parameters $\alpha = 10^0$, $y_f = 0.1$, $c_1 = 1.5\times10^{-2}$, $c_2 = 1.5\times10^{-3}$, $\phi = 1$, $S_L = 0.4129\ \mathrm{m\,s^{-1}}$ and $\Delta q_R = 2.7522\times10^6\ \mathrm{J\,kg^{-1}}$. Figure 3(*b*) plots the relative changes Ψ_1 and Ψ_2 for variation in the number of flame elements P for the same case. It is seen that the relative changes in both the maximum transient growth and the acoustic velocity at the flame location for the optimal initial condition are less than 3 % for $N = 100$ acoustic modes and $P = 500$ flame elements, respectively.

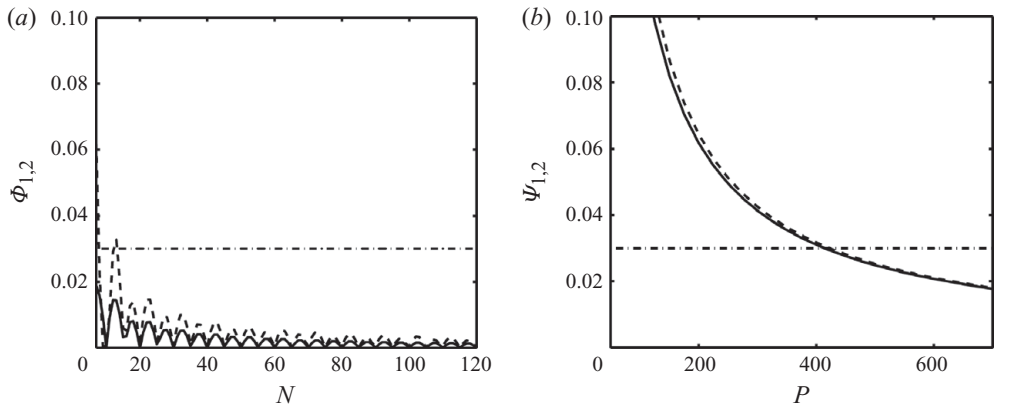

FIGURE 3. (*a*) Relative change in the average value of acoustic velocity at the flame for the optimal initial condition u'_f as Φ_1 (– – –) and relative change in maximum transient growth G_{max} as Φ_2 (———) with the number of acoustic modes N and 500 flame elements. (*b*) Relative change in u'_f as Ψ_1 (– – –) and in G_{max} as Ψ_2 (———) with the number of flame elements P and 100 acoustic modes at $\alpha = 10^\circ$, $y_f = 0.1$, $c_1 = 1.5 \times 10^{-2}$, $c_2 = 1.5 \times 10^{-3}$, $\phi = 1$, $S_L = 0.4129\,\mathrm{m\,s^{-1}}$ and $\Delta q_R = 2.7522 \times 10^6\,\mathrm{J\,kg^{-1}}$. In both the figures, (– · – · – · –) is the level indicating a relative change of 3 %.

Also, with 100 Galerkin modes retained in the expansion of acoustic variables, the jump in acoustic velocity across the heat source is sufficiently well resolved as shown in figure 7(*a*). With these choices, the set of ordinary differential equations given by (6.2), (6.5) and (6.8) is evolved in time using the matrix exponential of the linear operator (Hirsch, Smale & Devaney 2004) for linear analysis. In the nonlinear analysis, the set of equations given by (6.2), (6.3) and (6.11) is evolved with a time-marching technique using the Runge–Kutta third-order scheme with total variation diminishing (TVD) property (Jiang & Shu 1996). A Courant–Friedrichs–Lewy (CFL) number of 0.01 was used to determine the time step.

7. Results and discussions

7.1. *Quantification of transient growth*

In addition to the variables for acoustic velocity and pressure, the state vector of the self-evolving system consists of variables for the strengths of the monopole sources associated with the flame elements. The measure chosen in this paper to quantify transient growth contains contributions from the dilatation resulting from the fluctuating heat release rate in addition to the classical acoustic energy. The square of the L^2-norm of the state vector at time t gives the net energy of fluctuations $E(t)$. The fluctuation energy is normalized with its value at time $t = 0$ as given in (6.9). This normalized energy when maximized over all possible initial conditions and over all times is called maximum growth factor G_{max} and it represents the maximum possible amplification for the fluctuating energy of a given system. The optimal initial condition for maximum transient growth in a linear system can be obtained by singular value decomposition of the operator governing the linearized system. Evolution of the normalized energy for a linearly stable case from the corresponding optimal initial condition is shown in figure 4(*a*). The system configuration chosen is the same as for figure 3. The optimal initial condition, maximized over all times, is observed to undergo a transient amplification of 66.7 times the initial energy and attain this maximum amplification at $t_{max} = 3.3$.

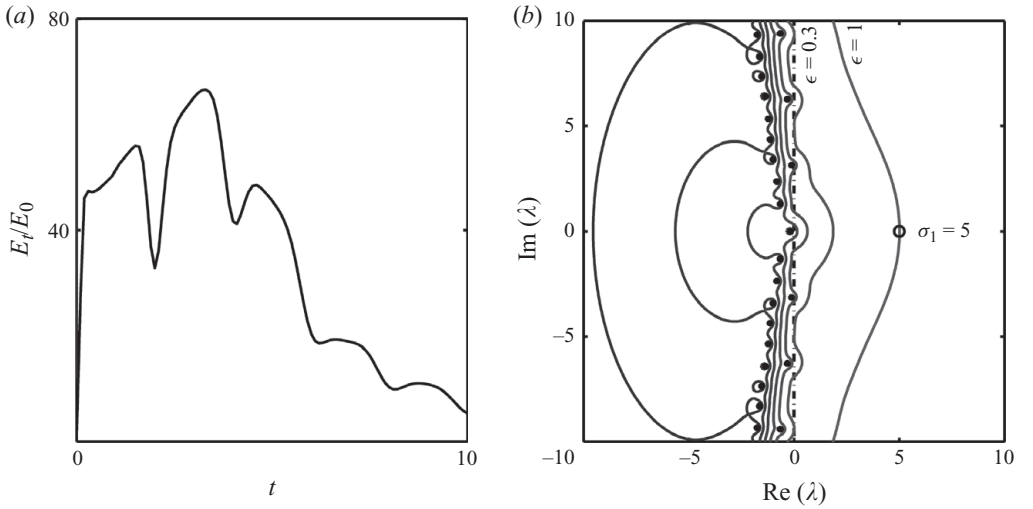

FIGURE 4. (*a*) Evolution of the ratio of energy at an instant E_t to the initial energy E_0 in the acoustic time scale t, for the optimal initial condition. (*b*) Pseudospectra of the linearized matrix of a linearly stable system with $\alpha = 10°$, $y_f = 0.08$, $c_1 = 0.135$, $c_2 = 0.015$, $\phi = 1$, $S_L = 0.4129\,\mathrm{m\,s^{-1}}$ and $\Delta q_R = 2.7522 \times 10^6\ \mathrm{J\,kg^{-1}}$.

For a non-normal system, the evolution of the system at finite time cannot be adequately characterized by the eigenvalues (λ) of the linearized system. In such cases, if $\boldsymbol{B}$ is the linear operator of the system, the eigenvalues enforce a bound on the growth factor $\|\exp(t\boldsymbol{B})\|$ only for $t \to \infty$. The normalized net energy of fluctuations is given by the square of the growth factor. Pseudospectra of the linearized operator can be analysed to obtain the magnitude of transient amplification of energy of the fluctuations. The time scale over which transient growth occurs can also be estimated from the pseudospectra of the linearized matrix.

The ϵ-pseudospectrum for the linear operator $\boldsymbol{B}$ is a set of points in the complex plane which are the eigenvalues of a perturbed matrix $(\boldsymbol{B}+\boldsymbol{T})$, such that the random perturbation $\boldsymbol{T}$ to the operator $\boldsymbol{B}$ satisfies the condition $||T|| < \epsilon$. On a given ϵ-pseudospectrum, the pseudospectral abscissa σ_ϵ gives the location of the point on the real axis with the largest value. If the value of σ_ϵ is positive, such that $(\sigma_\epsilon(\boldsymbol{B})/\epsilon) > 1$, then transient growth is indicated. The ratio of $(\sigma_\epsilon(\boldsymbol{B})/\epsilon)$ maximized over all ϵ gives the minimum value of transient growth possible. A lower bound on the magnitude of the transient growth can be given in terms of the Kreiss constant $\kappa(\boldsymbol{B})$ from the Kreiss matrix theorem as given below (Trefethen & Embree 2005):

$$\sup_{t\geqslant 0} \|\mathrm{e}^{t\boldsymbol{B}}\| \geqslant \sup_{\epsilon>0} \frac{\sigma_\epsilon(\boldsymbol{B})}{\epsilon} = \kappa(\boldsymbol{B}). \tag{7.1}$$

The upper bound on transient growth or $\varphi(\boldsymbol{B})$ for a matrix of dimension $(2N + P)$ is also given by the Kreiss matrix theorem in terms of $\kappa(\boldsymbol{B})$ as follows:

$$\|\mathrm{e}^{t\boldsymbol{B}}\| \leqslant \mathrm{e}(2N + P)\kappa(\boldsymbol{B}) = \varphi(\boldsymbol{B}). \tag{7.2}$$

In the case of a linearly unstable case, when z' is the location of the eigenvalue with the largest positive real part, exponential growth occurs within a time span of $1/\mathrm{Re}(z')$. In the case of a linearly stable system, the ϵ-pseudoeigenvalue of the system with the largest value determines the time span over which transient growth occurs.

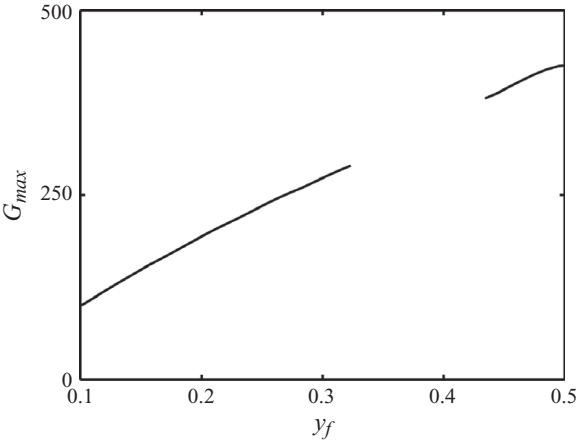

FIGURE 5. Variation of G_{max} with y_f for the system with $\alpha = 10^\circ$, $c_1 = 1.5 \times 10^{-2}$, $c_2 = 1.5 \times 10^{-3}$, $\phi = 1$, $S_L = 0.4129\,\mathrm{m\,s^{-1}}$ and $\Delta q_R = 2.7522 \times 10^6\ \mathrm{J\,kg^{-1}}$. Blank spaces indicate configurations for which the system is linearly unstable.

When the pseudospectral abscissa σ_ϵ is the ϵ-pseudoeigenvalue of the system with the largest real part, the system experiences a transient growth of the order of $\kappa(\boldsymbol{B})$ over a time span $1/\sigma_\epsilon$ (Trefethen & Embree 2005).

Thus, the pseudospectra of the linear matrix give us bounds for the evolution of normalized energy (E_t/E_0) at finite time. For the case of a premixed flame with $\phi = 1$ and flame angle of $\alpha = 10^\circ$, which is stabilized at $y_f = 0.08$, the pseudospectra of the system are given in figure 4(*b*). We see that the pseudospectra spill onto the right half-plane. The perturbation amplitude $\epsilon = 1$ gives a ratio of $\epsilon/||\boldsymbol{B}|| = 7.04 \times 10^{-4}$, which implies that the perturbations are very small compared to the norm of the linear operator. The pseudospectrum corresponding to $\epsilon = 1$ is seen to protrude by $\sigma_1 = 5$ units into the right half-plane. The ratio of the protrusion of the pseudospectra to the corresponding perturbation amplitude is greater than one, indicative of transient growth. This ratio when maximized over all perturbation amplitudes gives the Kreiss constant for this case as $\kappa(\boldsymbol{B}) = 6.4$, with $\sigma = 0.64$ and $\epsilon/||\boldsymbol{B}|| = 7.04 \times 10^{-5}$ for $\epsilon = 0.1$. The Kreiss constant sets the lower bound for transient amplification of energy to be $\kappa^2(\boldsymbol{B}) = 41$ from pseudospectra. The upper bound for transient growth is given as $\varphi(\boldsymbol{B}) = 7.7 \times 10^4$. The maximum value of normalized energy amplification is 66.7, as shown in figure 4(*a*), which falls within the bounds estimated from pseudospectra. The estimated time scale for transient growth from pseudospectra is $t_{max} = 1.6$, which is of the same order as the computed time for maximum growth, which is $t_{max} = 3.3$.

The variation of G_{max} with system parameters is obtained to quantify the effect of system parameters on the non-normality of the system. Significant system parameters considered are flame location y_f and flame angle α. The variation of G_{max} with the location of the flame is shown in figure 5 for a flame angle of $\alpha = 10^\circ$. It is seen that G_{max} increases with increase in y_f till the half duct length. The blank spaces in the distributions in figure 5 are configurations for which the system is linearly unstable. The system is linearly unstable for locations of the flame beyond the half duct length. The dependence of the growth factor on the flame angle is as shown in figure 6 for $y_f = 0.1$. The transient growth observed is stronger for elongated flames than for flatter flames. When α is small, i.e. for elongated flames, the convective term dominates the linear evolution of the flame front as given in (2.4). Increased

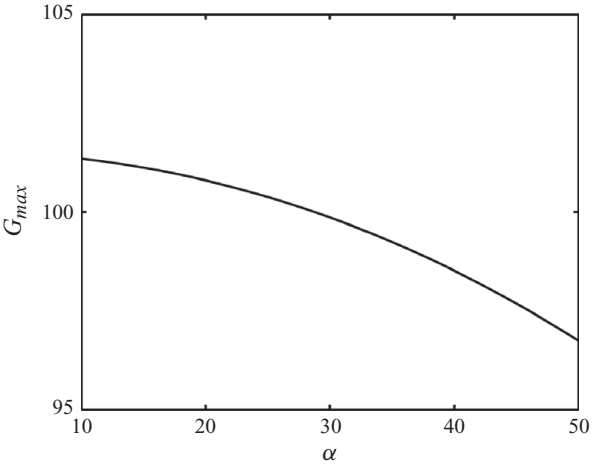

FIGURE 6. Variation of G_{max} with α for the system with $y_f = 0.1$, $c_1 = 1.5 \times 10^{-2}$, $c_2 = 1.5 \times 10^{-3}$, $\phi = 1$ with $S_L = 0.4129\,\mathrm{m\,s^{-1}}$ and $\Delta q_R = 2.7522 \times 10^6\ \mathrm{J\,kg^{-1}}$.

non-normality was observed with increased advection in the context of ducted diffusion flames by Balasubramanian & Sujith (2008*a*), who reported that the maximum growth factor was seen to increase with an increase in the Péclet number.

7.2. *Influence of internal flame dynamics*

In addition to the acoustic equations for momentum and energy, the dynamical system described in § 6.1 includes the evolution equation for the flame front in terms of the monopole strength averaged over the cross-sectional area of the duct. If the flame front is thought of as consisting of a number of small flame elements, the flame displacements at these points represent a large number of additional degrees of freedom which we refer to as the internal degrees of freedom of the flame front or internal flame dynamics. The linearized system of from (6.2), (6.5) and (6.8) can be written in matrix form as

$$\frac{\mathrm{d}\boldsymbol{\chi}}{\mathrm{d}t} = \boldsymbol{B}\boldsymbol{\chi} = \begin{pmatrix} \boldsymbol{C}_{2N\times 2N} & \boldsymbol{D}_{2N\times P} \\ \boldsymbol{E}_{P\times 2N} & \boldsymbol{F}_{P\times P} \end{pmatrix}_{(2N+P)\times(2N+P)} \boldsymbol{\chi}_{(2N+P)\times 1}. \tag{7.3}$$

Here, $\boldsymbol{\chi}$ is the state vector and $\boldsymbol{B}$ is the operator governing the linearized thermoacoustic system as expanded in Appendix B. The size of the linearized operator $\boldsymbol{B}$ is $(2N + P) \times (2N + P)$ for N number of acoustic modes and P number of points along the flame. The sub-matrix $\boldsymbol{C}$ is the linearized operator which governs the evolution of acoustic modes in the absence of a heat source and has the size $(2N \times 2N)$. Thus, the self-evolving thermoacoustic system has more degrees of freedom than just the number of acoustic modes. The sub-matrix $\boldsymbol{D}$ contains the effect of flame dynamics on the acoustic modes and $\boldsymbol{E}$ represents the acoustic driving term in the evolution of the monopole sources. The sub-matrix $\boldsymbol{F}$ represents the interaction between the monopole sources that represent the flame front.

The optimal initial condition can be obtained using singular-value decomposition (SVD) of the linear operator of the system (Schmid & Henningson 2001). The optimal initial condition was obtained for the case examined in figures 3 and 4. In the kinematic model considered, the heat release rate fluctuations are correlated to the monopole strength distribution along the flame. The optimal initial condition

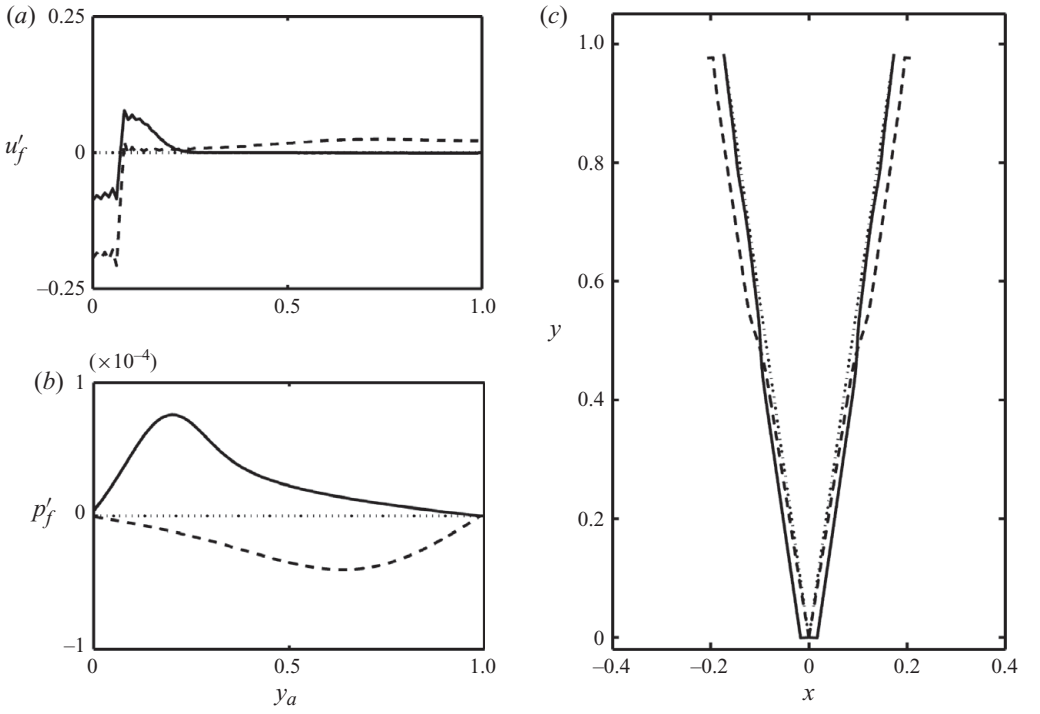

FIGURE 7. (*a*) Acoustic velocity field, (*b*) acoustic pressure field and (*c*) flame shape for the evolution of the optimal initial condition maximized over all times, with $E_t(0) = 1 \times 10^{-4}$ for $\alpha = 10^\circ$, $y_f = 0.08$, $c_1 = 0.135$, $c_2 = 0.015$, $\phi = 1$, $S_L = 0.4129\,\mathrm{m\,s^{-1}}$ and $\Delta q_R = 2.7522 \times 10^6$ $\mathrm{J\,kg^{-1}}$: · · · · · , the unperturbed state; ———, distribution for the optimal initial condition; – – ––, distribution at $t = t_{max} = 3.3$.

has significant projections onto the monopole strength distribution. The evolution from the optimum initial condition at different instances of time as seen through the projections on acoustic velocity, pressure and the displacement of the flame shape are shown in figure 7. The acoustic velocity and pressure distributions along the duct and the displacement of the flame shape for the optimal initial condition at time instances $t = 0$ and at time $t = t_{max} = 3.3$ are shown in figure 7(*a–c*). The acoustic velocity distribution in figure 7(*a*) shows a jump while the pressure distribution in figure 7(*b*) is continuous across the flame location.

Inclusion of the monopole strengths in the state space increases the number of degrees of freedom in the system from $(2N \times 2N)$ to $(2N+P) \times (2N+P)$. Traditionally, thermoacoustic instability has been analysed in terms of an acoustic model which is driven by combustion. In this traditional approach, a time lag model (Schuermans *et al.* 2004; Noiray *et al.* 2006) or a lumped model (Annaswamy *et al.* 1997) has been used to model the heat release rate fluctuations. The coupled system can have initial perturbations both in the acoustic variables and the position of the flame front.

When the flame front is modelled with a time lag model or as lumped model, it is not possible to prescribe an initial condition for the flame shape (monopole source strength distribution). In order to include the possibility of an initially perturbed flame shape (i.e. an initial non-zero monopole strength distribution), the variables corresponding to the monopole source strengths must be included in the state variables of the system. Inclusion of the monopole source strength variables in the state space retains the

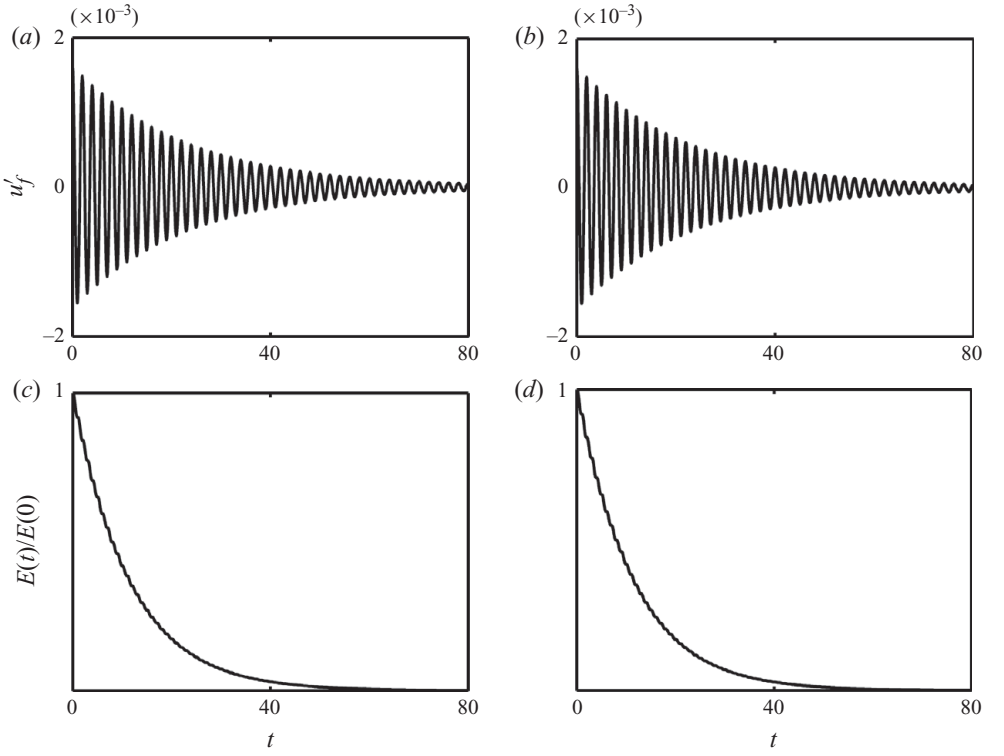

FIGURE 8. Evolution of acoustic velocity at the flame for (*a*) linearized system and (*b*) nonlinear system. Evolution of the normalized energy due to fluctuations $E(t)/E(0)$ for (*c*) linearized system and (*d*) nonlinear system. All evolutions are plotted along the acoustic time scale t. A purely acoustic initial condition with $u'_f(0) = 1.6 \times 10^{-3}$ and $E(0) = 4 \times 10^{-6}$ is seen to decay monotonically in both linear and nonlinear evolutions. The other system parameters are $\alpha = 10^{\circ}$, $y_f = 0.2$, $\phi = 0.8$, $c_1 = 2 \times 10^{-3}$, $c_2 = 2 \times 10^{-4}$, $S_L = 0.2782\,\mathrm{m\,s^{-1}}$ and $\Delta q_R = 2.2263 \times 10^6\ \mathrm{J\,kg^{-1}}$.

internal degrees of freedom of the flame front. This is particularly significant as the ability to predict transient growth in a non-normal system is affected by the degrees of freedom of the model (Trefethen & Embree 2005).

7.3. *Subcritical transition to instability*

A system that is predicted to be stable by classical linear stability theory can become nonlinearly unstable for large amplitudes of initial perturbation and reach a limit-cycle oscillation. Depending upon the amplitude of the initial perturbation, this type of stability transition is called subcritical transition to instability. The evolutions of acoustic velocity for the linearized and nonlinear systems are compared in figures 8(*a*) and 8(*b*) for the system configuration with $\alpha = 10^0$, $y_f = 0.2$, $c_1 = 2 \times 10^{-3}$, $c_2 = 2 \times 10^{-4}$, $\phi = 0.8$, $S_L = 0.2782\,\mathrm{m\,s^{-1}}$ and $\Delta q_R = 2.2263 \times 10^6\ \mathrm{J\,kg^{-1}}$. An initial condition purely in the acoustic variables with $\eta_1(0) = 0.002$, $\eta_i(0) = 0\ \forall\ i \neq 1$ and $\dot{\eta}_i(0) = 0\ \forall\ i = 1$ to N is given with an initial acoustic velocity of $u'_f(0) = 1.6 \times 10^{-3}$, and the initial energy due to fluctuations being $E(0) = 4 \times 10^{-6}$. The system is linearly stable and the linear evolution decays asymptotically without any transient growth. The nonlinear evolution also decays asymptotically.

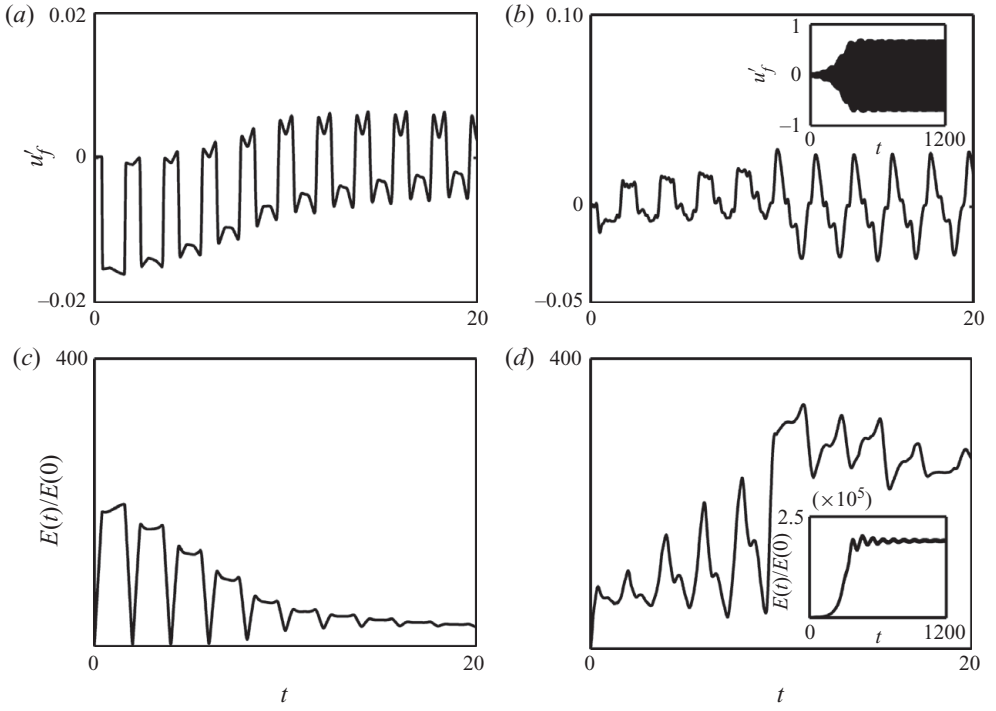

FIGURE 9. Evolution of acoustic velocity at the flame for (*a*) linearized system and (*b*) nonlinear system. Evolution of the energy due to fluctuations $E(t)/E(0)$ for (*c*) linearized system and (*d*) nonlinear system. All evolutions are plotted along the acoustic time scale t. The optimal initial condition with $u'_f(0) = 7.8 \times 10^{-5}$ and $E(0) = 4 \times 10^{-6}$ is seen to grow transiently and decay in the linear evolution. The nonlinear evolution reaches a limit cycle of amplitude $|u'_f|_{LC} = 0.67$. The other system parameters are $\alpha = 10°$, $y_f = 0.2$, $\phi = 0.8$, $c_1 = 2 \times 10^{-3}$, $c_2 = 2 \times 10^{-4}$, $S_L = 0.2782\,\mathrm{m\,s^{-1}}$ and $\Delta q_R = 2.2263 \times 10^6\,\mathrm{J\,kg^{-1}}$.

In a non-normal system, the transient growth obtained is dependent on the initial condition applied to the system. The initial condition which maximizes the transient amplification of energy is called the optimal initial condition. Figure 9 shows the evolution of the linear and nonlinear systems from the optimal initial condition for the same linearly stable case as shown in figure 8. The energy due to fluctuations is retained at the same value of $E(0) = 4 \times 10^{-6}$ as in figure 8. However, in this case the linear and nonlinear evolutions diverge within a short period of time. The linear evolution exhibits a transient growth of a factor of 197 in the energy due to fluctuations until $t_{max} = 1.5$ and then asymptotically decays. Initially, the nonlinear evolution undergoes lesser transient growth than the linear evolution but asymptotically reaches a limit cycle with $|u'_f|_{LC} = 0.67$. This is seen from the insets in figures 9(*b*) and 9(*d*).

From this example, it is evident that an initial condition with very small initial amplitude, if applied in an optimal manner, can cause transient growth in the energy of the system. If this transient growth is high enough for nonlinear effects to become significant, a system which is stable according to classical linear stability theory can become nonlinearly unstable. Therefore, in non-normal systems, even initial perturbations whose amplitudes are small enough for linearization to appear

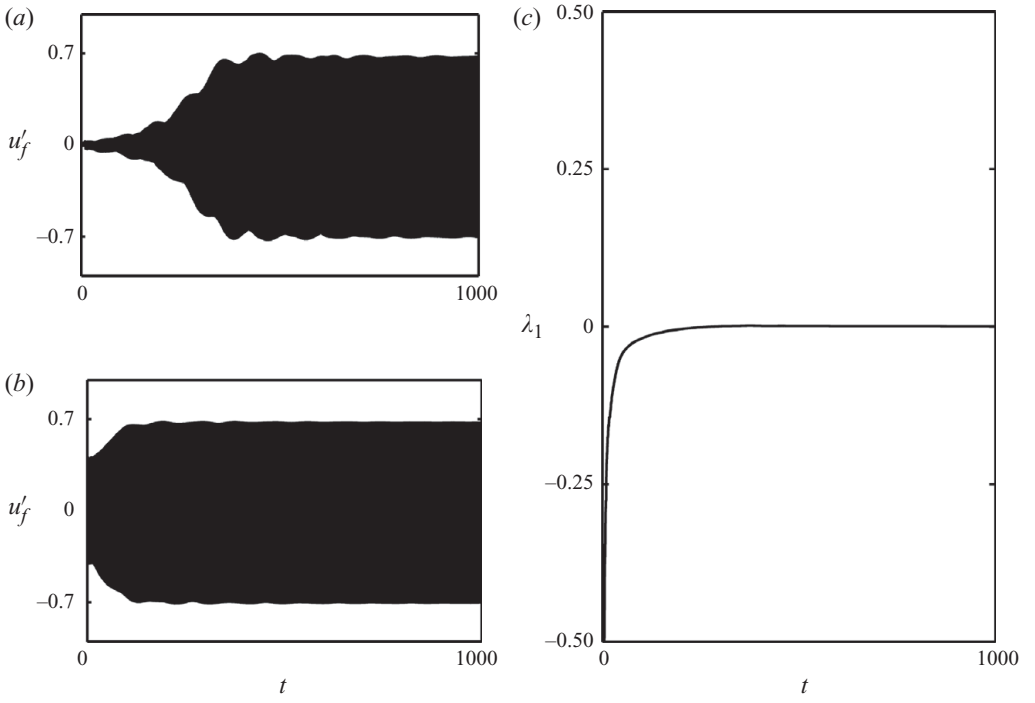

FIGURE 10. Nonlinear evolutions for $\alpha = 10^\circ$, $y_f = 0.2$, $\phi = 0.8$, $c_1 = 2 \times 10^{-3}$, $c_2 = 2 \times 10^{-4}$, $S_L = 0.2782\,\mathrm{m\,s^{-1}}$ and $\Delta q_R = 2.2263 \times 10^6\ \mathrm{J\,kg^{-1}}$ for initial conditions with (*a*) optimal initial condition with $u'_f(0) = 7.8 \times 10^{-5}$, (*b*) initial condition with $u'_f(0) = 0.40$, (*c*) rate of separation of the two evolutions given in (*a*) and (*b*). All evolutions are plotted along the acoustic time scale t.

apparently legitimate, can cause the nonlinear evolution to reach self-sustaining oscillations.

For the linearly stable system shown in figures 8 and 9, two nonlinear evolutions which differ only in the value of the initial condition are shown in figures 10(*a*) and 10(*b*). The two evolutions evolve to the same limit cycle even when all eigenvalues are stable. This asymptotic behaviour of the nonlinear evolution is characterized as a limit cycle using the Lyapunov exponent (Wolf *et al.* 1985). The Lyapunov exponent λ_1 is a measure of the rate at which two nearby trajectories asymptotically diverge from each other. A limit cycle is obtained when the Lyapunov exponent between the two evolutions goes to zero. In figure 10(*c*), it is seen that the value of the Lyapunov exponent asymptotically converges to zero, which confirms that the asymptotic state is a limit cycle.

7.4. *Evolution of an initially decaying system*

Nonlinear evolution of acoustic velocity for a linearly stable system is shown in figure 11(*a*). It shows an initial decay with a higher frequency and then a shift to a dominant mode of lower frequency. Despite the initial decay, the evolution reaches a self-repeating limit cycle asymptotically. An analysis of the frequency content of the evolution during different intervals of time is performed in order to identify the dominant modes. Enlarged plots of the acoustic evolution are shown in figure 11(*b*–). Corresponding plots of amplitude $|A|$ versus frequency f are shown in figure 11(*e*–*g*). Non-dimensional frequency for the fundamental mode of the duct is 0.5 with higher

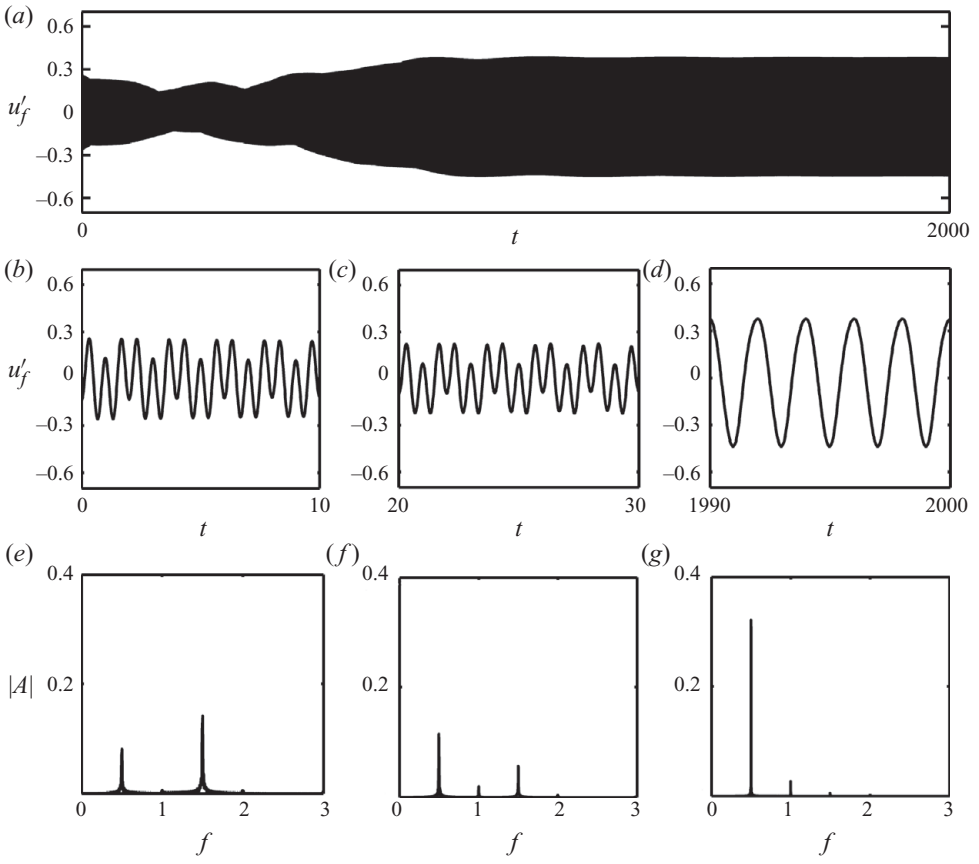

FIGURE 11. (*a*) Evolution of acoustic velocity with $u'_f(0) = -0.14$ to a limit cycle of amplitude $|u'_f|_{LC} = 0.41$ plotted along the acoustic time scale t. Enlarged views of acoustic velocity evolution between (*b*) $0 < t \leqslant 10$, (*c*) $20 < t \leqslant 30$ and (*d*) $1990 < t \leqslant 2000$. FFT of the signal between (*e*) $0 < t \leqslant 10$, (*f*) $10 < t \leqslant 30$ and (*g*) $30 < t \leqslant 2000$ showing change in the dominant frequency during evolution. System parameters for the linearly stable system are $\alpha = 10^\circ$, $y_f = 0.2$, $\phi = 0.6$, $c_1 = 2 \times 10^{-3}$, $c_2 = 2 \times 10^{-4}$, $S_L = 0.1231\ \mathrm{m\,s^{-1}}$ and $\Delta q_R = 1.6885 \times 10^6\ \mathrm{J\,kg^{-1}}$.

modes having multiples of this fundamental frequency. Figure 11(*e*) shows that initially the third mode is dominant during time $0 < t \leqslant 10$. Comparable amplitudes for the first and third modes are obtained for the evolution between $10 < t \leqslant 30$ in figure 11(*f*) and then the first mode is seen to dominate the evolution from figure 11(*g*). Transfer of energy between modes causes the shift in dominant mode during evolution.

The evolution of the phase θ between acoustic pressure and the heat release rate oscillations is shown in figure 12. In a self-evolving thermoacoustic system, the phase between acoustic pressure and the heat release rate fluctuations is free to evolve and change with time. From the inset in figure 12, it is observed that θ initially remains at acute angles indicative of driving. However, later it evolves to obtuse angles, which is indicative of damping and remains at these obtuse values for many cycles. Finally the evolution of the phase settles at an acute angle such that the driving from the unsteady heat release rate balances the damping present in the system as shown by the asymptotic behaviour of the evolution of the phase. The phase between heat release

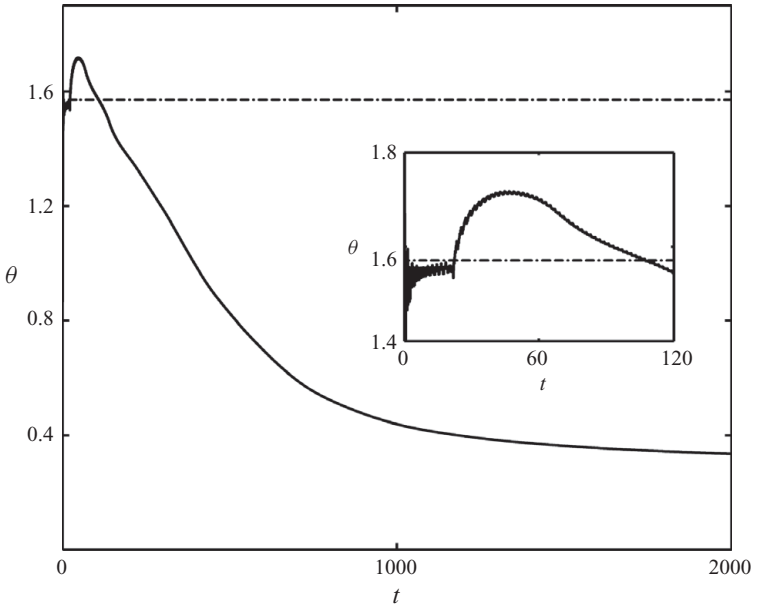

FIGURE 12. Evolution of the phase angle θ between acoustic pressure and heat release rate fluctuations for linearly stable system with $\alpha = 10^{\circ}$, $y_f = 0.2$, $\phi = 0.6$, $c_1 = 2 \times 10^{-3}$, $c_2 = 2 \times 10^{-4}$, $S_L = 0.1231\,\mathrm{m\,s^{-1}}$ and $\Delta q_R = 1.6885 \times 10^6\,\mathrm{J\,kg^{-1}}$ for the evolution shown in figure 11(*d*). The inset shows short-term evolution of the phase angle θ. Evolutions are plotted along the acoustic time scale t.

rate fluctuations and acoustic pressure is therefore only an indicator of stability that is local in time and cannot be used to predict the asymptotic stability of the system.

8. Conclusions

The non-normal nature of thermoacoustic interaction in ducted premixed flames is characterized. The unsteady heat release rate from the flame front acts as a source of unsteady dilatation. Therefore, the laminar flame front is modelled as a distribution of monopole sources of sound. The energy due to fluctuations in the premixed flame–acoustic system includes the energy due to the monopole sources in addition to the fluctuations in acoustic pressure and velocity. This total energy due to fluctuations is used as a measure of non-normal transient growth. Parametric study of the variation in transient growth due to change in parameters such as flame angle and flame location is conducted. Larger transient growth is observed when convective effects dominate.

Traditionally, thermoacoustic instabilities have been analysed in terms of an acoustic model which is driven by combustion. However, the thermoacoustic system has more degrees of freedom than the number of acoustic modes. These additional degrees of freedom represent the internal degrees of freedom of the flame front or the internal flame dynamics. In addition to the acoustic variables, the optimal initial condition for a linearly stable thermoacoustic system displays significant projections along the monopole source strength distribution or the heat release rate variables. In order to accurately capture the non-normal effects, the internal degrees of the flame front must be accounted for in the model for the evolution of the thermoacoustic system.

Subcritical transition to instability has been thought of as being caused by a large-amplitude initial perturbation to a linearly stable system. In a linearly stable case, even a small but finite-amplitude initial perturbation is shown to reach limit cycle. In contrast to the same case, an initial condition purely in acoustic variables is seen to monotonically decay. Therefore, for non-normal systems, even initial perturbations whose amplitudes are small enough for linearization to appear apparently legitimate can cause the nonlinear evolution to reach self-sustaining oscillations.

Nonlinear evolutions can display dominant mode change during evolution for a linearly stable case for an initially decaying evolution. For this initially decaying evolution, the phase between acoustic pressure and the heat release rate fluctuations was shown to drift over many cycles between values indicative of driving and damping before settling to a constant value. Therefore, the phase between acoustic pressure and heat release rate fluctuations is an indicator of stability that is local in time and cannot be used to determine the asymptotic stability of a thermoacoustic system.

This work was funded by the Department of Science and Technology (DST) of the Government of India.

Appendix A. Implementation of WENO scheme

The high-resolution WENO scheme uses a six-point stencil formed of three sub-stencils each with four points. It will therefore give fifth-order accuracy in the smooth regions and third-order accuracy in the discontinuous regions. Implementation of WENO assumes that the function $\xi'(X,t)$ is continuous, with piece-wise smooth spatial derivatives, i.e. the discontinuities in the spatial derivative are isolated. The domain can then be discretized with X_i being the set of uniform discretization points along the flame front with an equidistant spacing of ΔX. If $\xi_i = \xi(X_i)$ and

$$\Delta^+\xi_k = \xi_{k+1} - \xi_k, \qquad \Delta^-\xi_k = \xi_k - \xi_{k-1} \tag{A 1}$$

are as defined above, then the approximation for the spatial derivative at the ith location using a left biased stencil which is written in (A 2) and is given by a weighted average of the values due to the individual stencils 0, 1 and 2 shown in (A 3):

$$\frac{\partial \xi'}{\partial X} = \xi^-_{X,i}, \tag{A 2}$$

$$\xi^-_{X,i} = w_{0,NL}\xi^{-,0}_{X,i} + w_{1,NL}\xi^{-,1}_{X,i} + w_{2,NL}\xi^{-,2}_{X,i}, \tag{A 3}$$

with

$$\xi^{-,0}_{X,i} = \frac{1}{3}\frac{\Delta^+\xi_{i-3}}{\Delta X} - \frac{7}{6}\frac{\Delta^+\xi_{i-2}}{\Delta X} + \frac{11}{6}\frac{\Delta^+\xi_{i-1}}{\Delta X}, \tag{A 4}$$

$$\xi^{-,1}_{X,i} = -\frac{1}{6}\frac{\Delta^+\xi_{i-2}}{\Delta X} + \frac{5}{6}\frac{\Delta^+\xi_{i-1}}{\Delta X} + \frac{1}{3}\frac{\Delta^+\xi_{i}}{\Delta X}, \tag{A 5}$$

$$\xi^{-,2}_{X,i} = \frac{1}{3}\frac{\Delta^+\xi_{i-1}}{\Delta X} + \frac{5}{6}\frac{\Delta^+\xi_{i}}{\Delta X} - \frac{1}{6}\frac{\Delta^+\xi_{i+1}}{\Delta X}, \tag{A 6}$$

where $\xi^{-,s}_{X,i}$ is the third-order approximation to $\xi^-_{X,i}$ on the sth sub-stencil. In an ENO scheme, one of the $\xi^{-,s}_{X,i}$ would be chosen based on the relative smoothness of the sub-stencil. The nonlinear weight of the derivative calculated in a sub-stencil depends on the smoothness of the function derivative in that sub-stencil. The modified smoothness

indicators are given in (A 7)–(A 9) (Jiang & Shu 1996; Zhang & Shu 2007):

$$IS_0 = (\xi_{i-2} - 4\xi_{i-1} + 3\xi_i)^2, \tag{A 7}$$

$$IS_1 = (\xi_{i-1} - \xi_{i+1})^2, \tag{A 8}$$

$$IS_2 = (3\xi_i - 4\xi_{i+1} + \xi_{i+2})^2, \tag{A 9}$$

which are then used to calculate the nonlinear weights as given below, with typical values for $p = 2$ and $\epsilon = 10^{-6}$,

$$\mu_s = \frac{w_{s,L}}{(\varepsilon + IS_s)^r}, \tag{A 10}$$

$$w_{s,NL} = \frac{\mu_s}{\sum_{s=0}^{2} \mu_s}. \tag{A 11}$$

Here the linear weights $w_{s,L}$ for the sth sub-stencil at point i are made to satisfy the consistency condition, such that

$$\sum_{s=0}^{2} w_{s,L} = 1. \tag{A 12}$$

When the linear weights are $w_{0,L} = 0.3$, $w_{1,L} = 0.6$ and $w_{2,L} = 0.1$, we obtain the fifth-order-accurate solution in the smooth regions. While using WENO with a left biased stencil, we require derivative values for the first three points and the last two points. The appropriate fifth-order-accurate explicit scheme is used to calculate the first derivative of the function values at boundary cells (Zhong 1998).

Appendix B. Linear operator

If the matrix governing the linearized thermoacoustic system as given in the set of (6.2), (6.5) and (6.8) is $\boldsymbol{B}$, they can be written as given in (B 1) for the state vector $\boldsymbol{\chi}$ in (B 2). Then the sub-matrices can be expanded as given in (B 3) to (B 6):

$$\boldsymbol{B} = \begin{pmatrix} \boldsymbol{C}_{2N\times 2N} & \boldsymbol{D}_{2N\times P} \\ \boldsymbol{E}_{P\times 2N} & \boldsymbol{F}_{P\times P} \end{pmatrix}_{(2N+P)\times(2N+P)}, \tag{B 1}$$

$$\boldsymbol{\chi} = \begin{pmatrix} \eta_1 \\ \dot{\eta}_1/\pi \\ \eta_2 \\ \dot{\eta}_2/2\pi \\ . \\ . \\ \dot{\eta}_N/N\pi \\ H_1 \\ H_2 \\ . \\ . \\ H_P \end{pmatrix}_{(2N+P)\times 1}, \tag{B 2}$$

$$\boldsymbol{C} = \begin{pmatrix} 0 & \pi & . & . & . & . & . & . \\ -\pi & -2\zeta_1 k_1 & . & . & . & . & . & . \\ . & . & 0 & 2\pi & . & . & . & . \\ . & . & -2\pi & -2\zeta_2 k_2 & . & . & . & . \\ . & . & . & . & . & . & . & . \\ & & & & & & 0 & N\pi \\ . & . & . & . & & . & -N\pi & -2\zeta_N k_N \end{pmatrix}_{2N\times 2N}, \tag{B 3}$$

$$\boldsymbol{D} = -\sqrt{2}\begin{pmatrix} 0 & 0 & . & . & 0 \\ 0 & \sin(\pi y_f) & . & . & 2\sin(\pi y_f) \\ 0 & 0 & . & . & 0 \\ 0 & \sin(2\pi y_f) & . & . & 2\sin(2\pi y_f) \\ 0 & 0 & . & . & 0 \\ 0 & \sin(3\pi y_f) & . & . & 2\sin(3\pi y_f) \\ 0 & 0 & . & . & 0 \\ . & . & . & . & . \\ . & . & . & . & . \\ 0 & 0 & . & . & 0 \\ 0 & \sin(N\pi y_f) & . & . & 2\sin(N\pi y_f) \end{pmatrix}_{2N\times P}, \tag{B 4}$$

$$\boldsymbol{E} = \begin{pmatrix} 0 & 0 & 0 & 0 & . & . & 0 & 0 \\ \theta_1\cos(\pi y_f) & 0 & \theta_1\cos(2\pi y_f) & 0 & . & . & \theta_1\cos(N\pi y_f) & 0 \\ . & . & . & . & . & . & . & . \\ . & . & . & . & . & . & . & . \\ \theta_1\cos(\pi y_f)/2 & 0 & \theta_1\cos(2\pi y_f)/2 & 0 & . & . & \theta_1\cos(N\pi y_f)/2 & 0 \end{pmatrix}_{P\times 2N}, \tag{B 5}$$

$$\boldsymbol{F} = \begin{pmatrix} 0 & . & . & . & . & . & . & . \\ 0 & -\theta_2 & . & . & . & . & . & . \\ . & \theta_2 & -\theta_2 & . & . & . & . & . \\ . & . & \theta_2 & -\theta_2 & . & . & . & . \\ . & . & . & . & . & . & . & . \\ . & . & . & . & . & . & . & . \\ . & . & . & . & . & . & \theta_2 & -\theta_2 \end{pmatrix}_{P\times P}. \tag{B 6}$$

Here H_i corresponds to the monopole strength averaged over the cross-sectional area of the duct and the values of constants θ_1 and θ_2 are defined in (6.8). The spatial derivative is approximated with the first-order backward-difference formula and the integration for the source term is approximated with a trapezoidal integration over all points along the flame front.

REFERENCES

Annaswamy, A. M., Fleifil, M., Hathout, J. P. & Ghoneim, A. F. 1997 Impact of linear coupling on the design of active controllers for the thermoacoustic instability. *Combust. Sci. Technol.* **128**, 131–180.

Bakas, N. A. 2009 Mechanisms underlying transient growth of planar perturbations in unbounded compressible shear flow. *J. Fluid Mech.* **639**, 479–507.

Balasubramanian, K. & Sujith, R. I. 2008*a* Non-normality and nonlinearity in combustion acoustic interaction in diffusion flames. *J. Fluid Mech.* **594**, 29–57.

Balasubramanian, K. & Sujith, R. I. 2008*b* Thermoacoustic instability in a Rijke tube: nonnormality and nonlinearity. *Phys. Fluids* **20**, 044103.

Bloomshield, F. S., Crump, J. E., Mathes, H. B., Stalnaker, R. A. & Beckstead, M. W. 1997 Nonlinear stability testing of full scale tactical motors. *J. Propul. Power* **13** (3), 356–366.

Boyer, L. & Quinard, J. 1990 On the dynamics of anchored flames. *Combust. Flame* **82**, 51–65.

Candel, S. 2002 Combustion dynamics and control: progress and challenges. *Proc. Combust. Inst.* **29**, 1–28.

Chagelishvili, G. D., Rogava, A. D. & Segal, I. N. 1994 Hydrodynamic stability of compressible plane Couette flow. *Phys. Rev.* E **50**, 4283–4285.

Chu, B. T. 1964 On the energy transfer to small disturbances in fluid flow (Part I). *Acta Mechanica* **1** (3), 215–234.

Chu, B. T. & Kovasznay, L. S. G. 1957 Non-linear interactions in a viscous heat-conducting compressible gas. *J. Fluid Mech.* **3**, 494–514.

Coats, C. M. 1996 Coherent structures in combustion. *Prog. Energy Combust. Sci.* **22**, 427–509.

Dowling, A. P. 1997 Nonlinear self-excited oscillations of a ducted flame. *J. Fluid Mech.* **346**, 271–290.

Dowling, A. P. 1999 A kinematic model of a ducted flame. *J. Fluid Mech.* **394**, 51–72.

Dowling, A. P. & Morgens, A. S. 2005 Feedback control of combustion oscillations. *Annu. Rev. Fluid Mech.* **37**, 151–182.

Dowling, A. P. & Williams, F. W. 1983 *Sound and Sources of Sound*. Ellis Horwood.

Farrell, B. F. & Ioannou, P. J. 2000 Transient and asymptotic growth of two-dimensional perturbations in viscous compressible shear flow. *Phys. Fluids* **12**, 3021–3028.

Fleifil, M., Annaswamy, A., Ghoneim, Z. & Ghoneim, A. 1996 Response of a laminar premixed flame to flow oscillations: a kinematic model and thermoacoustic instability results. *Combust. Flame* **106**, 487–510.

Giauque, A., Poinsot, T., Brear, M. J. & Nicoud, F. 2006 Budget of disturbance energy in gaseous reacting flows. In *Proc. 2006 Summer Program*, Center for Turbulence Research, Stanford University.

Hirsch, M. W., Smale, S. & Devaney, R. L. 2004 *Differential Equations, Dynamical Systems and an Introduction to Chaos*, 2nd edn. Academic Press/Elsevier.

Howe, M. S. 2003 *Theory of Vortex Sound*. Cambridge University Press.

Jiang, G. S. & Shu, C. W. 1996 Efficient implementation of weighted WENO schemes. *J. Comput. Phys.* **126**, 202–228.

Juniper, M. P. 2010 Triggering in the horizontal Rijke tube: non-normality, transient growth and bypass transition. *J. Fluid Mech.* **667**, 272–308.

van Kampen, J. F. 2006 Acoustic pressure oscillations induced by confined turbulent premixed natural gas flames. PhD thesis, University of Twente.

Karimi, N., Brear, M., Jin, S.-H. & Monty, J. P. 2009 Linear and nonlinear forced response of conical, ducted, laminar, premixed flames. *Combust. Flame* **156**, 2201–2212.

Kerstein, A. R., Ashurst, W. T. & Williams, F. A. 1988 Field equation for interface propagation in an unsteady homogenous flow field. *Phys. Rev.* A **37** (7), 2728–2731.

Lieuwen, T. 2003 Modeling premixed combustion–acoustic wave interactions: a review. *J. Propul. Power* **19–5**, 765–781.

Lieuwen, T. 2005 Nonlinear kinematic response of premixed flames to harmonic velocity disturbances. *Proc. Combust. Inst.* **30**, 1725–1732.

Lieuwen, T. & Zinn, B. T. 1998 The role of equivalence ratio oscillations in driving combustion instabilities in low NO_X gas turbines. In *27th Intl Symp. on Combustion*, pp. 1809–1816.

Lighthill, M. J. 1952 On sound generated aerodynamically. I. General theory. *Proc. R. Soc. Lond.* A **211**, 564–587.

Mack, L. M. 1969 Boundary-layer stability theory. *Tech. Rep. Doc.* 900–277. JPL.

Mariappan, S. & Sujith, R. I. 2010 Thermoacoustic instability in a solid rocket motor: non-normality and nonlinear instabilities. *J. Fluid Mech.* **653**, 1–33.

Markstein, G. H. 1964 *Nonsteady Flame Propagation*. Pergamon.

Matveev, K. 2003*a* A model for combustion instability involving vortex shedding. *Combust. Sci. Technol.* **175** (6), 1059–1083.

Matveev, K. 2003*b* Thermoacoustic instabilities in the Rijke tube: experiments and modeling. PhD thesis, California Institute of Technology, Pasadena.

McManus, K., Poinsot, T. & Candel, S. 1993 A review of active control of combustion instabilities. *Prog. Energy Combust. Sci.* **19**, 1–29.

Meirovitch, L. 1967 *Analytical Methods in Vibration*. Macmillan.

Morfey, C. L. 1971 Sound transmission and generation in ducts with flow. *J. Sound Vib.* **14** (1), 37–55.

Morse, P. M. & Ingard, K. U. 1968 *Theoretical Acoustics*. McGraw-Hill.

Myers, M. K. 1991 Transport of energy by disturbances in arbitrary steady flows. *J. Fluid Mech.* **226**, 383–400.

Nicoud, F., Benoit, A., Sensiau, C. & Poinsot, T. 2007 Acoustic modes in combustors with complex impedances and multidimensional active flames. *AIAA J.* **45** (2), 426–441.

Nicoud, F. & Poinsot, T. 2005 Thermoacoustic instabilities: should the Rayleigh criterion be extended to include entropy changes? *Combust. Flame* **142**, 153–159.

Nicoud, F. & Wieczorek, K. 2009 About the zero Mach number assumption in the calculation of thermoacoustic instabilities. *Intl J. Spray Combust. Dyn.* **1** (1), 67–111.

Noiray, N., Durox, D., Schuller, T. & Candel, S. 2006 Self-induced instabilities of premixed flames in a multiple injection configuration. *Combust. Flame* **145**, 435–446.

Noiray, N., Durox, D., Schuller, T. & Candel, S. 2008 A unified framework for nonlinear combustion instability analysis based on the flame describing function. *J. Fluid Mech.* **615**, 139–167.

Poinsot, T. J., Trouve, A. C., Veynante, D. P., Candel, S. M. & Esposito, E. J. 1987 Vortex-driven acoustically coupled combustion instabilities. *J. Fluid Mech.* **177**, 265–292.

Rienstra, S. W. & Hirschberg, A. 2008 An introduction to acoustics. *IWDE Rep.* 92–06.

Schmid, P. J. & Henningson, D. S. 2001 *Stability and Transition in Shear Flows*. Springer.

Schuermans, B., Bellucci, V., Guethe, F., Meili, F., Flohr, P. & Paschereit, O. 2004 A detailed analysis of thermoacoustic interaction mechanisms in a turbulent premixed flame. In *Proc. ASME Turbo Expo 2004: Power for Land, Sea, and Air, 14–17 June*, Vienna, Austria.

Schuller, T., Durox, D. & Candel, S. 2003 A unified model for the prediction of laminar flame transfer functions: comparisons between conical and *v*-flame dynamics. *Combust. Flame* **134**, 21–34.

Sterling, J. D. & Zukoski, E. E. 1991 Nonlinear dynamics of laboratory combustor pressure oscillations. *Combust. Sci. Technol.* **77**, 225–238.

Subramanian, P., Mariappan, S., Wahi, P. & Sujith, R. I. 2010 Bifurcation analysis of thermoacoustic instability in a horizontal Rijke tube. *Intl J. Combust. Spray Dyn.* **2** (4), 325–356.

Trefethen, L. N. & Embree, M. 2005 *Spectra and Pseudospectra: The Behavior of Nonnormal Matrices and Operator*. Princeton University Press.

Wicker, J. M., Greene, W. D., Kin, S.-I. & Yang, V. 1996 Triggering of longitudinal combustion instabilities in rocket motors: nonlinear combustion response. *J. Propul. Power* **12**, 1148–1158.

Wolf, A., Swift, J. B., Swinney, H. L. & Vastano, J. A. 1985 Determining Lyapunov exponents from a time series. *Physica* D **16**, 285–317.

Wu, X., Wang, M., Moin, P. & Peters. N. 2003 Combustion instability due to nonlinear interaction between sound and flame. *J. Fluid Mech.* **497**, 23–53.

You, D., Huang, Y. & Yang. V. 2005 A generalized model of acoustic response of turbulent premixed flame and its application to gas-turbine combustion instability analysis. *Combust. Sci. Technol.* **177**, 1109–1150.

Zhang, S. & Shu, C. W. 2007 A new smoothness indicator for the WENO schemes and its effects on the convergence to steady state solutions. *J. Sci. Comput.* **31**, 273–305.

Zhong, X. 1998 Upwind compact and explicit high order finite difference schemes for direct numerical simulation of high speed flows. *J. Comput. Phys.* **144** (2), 662–709.

Zinn, B. T. & Lores, M. E. 1971 Application of the Galerkin method in the solution of non-linear axial combustion instability problems in liquid rockets. *Combust. Sci. Technol.* **4** (1), 269–278.